Effect of Biofilm Formation on the Sorption of Per- and Polyfluoroalkyl Substances to Colloidal Activated Carbon

by

Erica Lynne Moran

A thesis

presented to the University of Waterloo

in fulfilment of the

thesis requirement for the degree of

Master of Applied Science

in

Civil Engineering

Waterloo, Ontario, Canada, 2025

© Erica Lynne Moran 2025

Author's Declaration

I hereby declare that I am the sole author of this thesis. This is a true copy of the thesis, including any required final revisions, as accepted by my examiners. I understand that my thesis may be made electronically available to the public.

Abstract

Per- and polyfluoroalkyl substances (PFAS) are a class of contaminants that have garnered increasing concern due to their widespread presence and harmful effects on humans and ecosystems. PFAS enter the environment via many different pathways, with the release of PFAS-containing aqueous firefighting foams being a major source of groundwater contamination. Because PFAS are highly resistant to most chemical and biological degradation processes, they are currently removed from groundwater mainly by ex-situ adsorption, which is expensive and energy intensive.

Recently, activated carbon (AC) permeable reactive barriers (PRBs) have been proposed and used in-situ to limit the downgradient migration of PFAS by groundwater. AC PRBs are created by injecting powdered activated carbon (PAC) or colloidal activated carbon (CAC) into the subsurface to generate a stationary zone that removes PFAS by adsorption. As with any adsorption technology, however, PFAS breakthrough will occur once adsorptive sites in the barrier are exhausted. To improve our understanding of the ability of AC PRBs to adsorb PFAS and their longevity, there is a need for research that evaluates the adsorption of PFAS on AC and the factors affecting this process. The research reported in this thesis focused on one potential influencing factor, namely biofilm. Specifically, the objectives of this study were first, to evaluate if a biofilm can form on small (<5 μm) CAC particles, and second, to examine the impact that biofilm may have on the adsorption of PFAS to CAC.

To address the first objective, the growth of *Pseudomonas putida* (*P.putida*), an aerobic bacterium, in the absence of particulate and in the presence of either CAC or fine silica was investigated. *P.putida* was selected because it has been shown to readily form a biofilm, is not infectious to humans, is commonly found in the environment, and has applications in the

bioremediation of organic contaminants. Analyses of the bacterial samples by confocal laser scanning microscopy (CLSM) indicated that the bacteria remained planktonic when no particulate was present but formed a biofilm consisting of cells and CAC or sand particles held together by extracellular polymeric substances (EPS). Over seven days of growth, the biofilm formed on CAC increased in thickness and decreased in roughness as it developed and formed more cohesive structures. Results suggest that *P.putida* is capable of forming a biofilm on CAC particles. Rather than the classical depiction of a biofilm adhered to a single surface, the *P.putida* biofilm was formed on an aggregate of CAC particles, which were held together by EPS.

To address the second objective, the adsorption of perfluoroctane sulfonate (PFOS, a hydrophobic PFAS) and perfluoropentane carboxylate (PFPeA, a hydrophilic PFAS) on virgin and biofilm-coated CAC was investigated. *P.putida* was grown in the presence of CAC, and either PFOS or PFPeA was added to the microcosms once a biofilm was formed. Because the adsorption of PFAS to CAC is known to be impacted by the presence of dissolved organic carbon (DOC), experiments were also conducted to determine the impact of broth (used for culture growth) concentration on the extent of PFAS sorption to CAC and the development of the biofilm.

In the experiments without bacteria, the amount of PFOS adsorbed to CAC decreased as the concentration of broth was increased. The relationship between aqueous and sorbed PFOS could not be described by a linear, Freundlich, or Langmuir isotherm model, likely due to competitive sorption between the DOC present in the broth and PFOS. In the experiments with *P.putida*, it was observed that as the broth concentration increased, the biofilm became thicker and smoother, as the additional broth appeared to have aided biofilm development. Subsequent experiments, conducted with 3 mg/L broth and 80 mg/L broth (which represented high and low DOC concentrations, respectively), revealed that the majority of PFOS sorption on virgin and biofilm-

coated CAC occurred during the first three days, and the biofilm resulted in a decrease in PFOS adsorption. This decreased adsorption is presumed to be due to biofilm blocking sorption sites. For PFPeA, limited sorption occurred, and no significant difference was observed between the amount adsorbed in the bacteria-free CAC and *P.putida*-containing CAC systems. The difference in sorption between PFOS and PFPeA was attributed to decreased hydrophobic interactions between CAC and the shorter fluorinated tail of PFPeA.

The results of this study improve our understanding of how biofilm may impact CAC PRBs implemented for the management of PFAS. Biofilm can form on cell-sized particles and, as a result, may reduce the adsorption of long-chain compounds, such as PFOS. The effect of biofilm on the adsorption of short-chain compounds, such as PFPeA, may be less prominent than for PFOS, as the extent of sorption is comparatively limited. Further investigation is required to evaluate the impacts of biofilm on CAC sorption of other PFAS, the interactions of biofilm with other groundwater parameters, and the extent to which biofilm plays a role in the longevity of CAC PRBs in column or field scale studies.

Acknowledgements

Thank you to my supervisors, Dr. Anh Pham and Dr. Neil R. Thomson for the guidance and expertise that made this work possible.

Financial support for this study was provided by the Natural Sciences and Engineering Research Council of Canada (NSERC, Discovery Grant RGPIN-2022-03005 awarded to Dr. Anh Pham).

Thank you to Mark Merlau and Mark Sobon, for helping get my experiments up and running. Additionally, thank you to Griselda Raquel Rocha Díaz de León and Dr. Courtney Toth for answering my many microbiology questions.

Thank you to the members of Dr. Pham's research group (past and present), Ali Can Ozelcaglayan, Alannah Taylor, Andrew Uramowski, Blessing Medon, Bill McLaren, Celine Vandenberg, Luke Vandenberg, Madeline Myles, Dr. Seyfollah Gilak Hakimabadi, and Dr. Hak-Hyeon Kim for your kindness, friendship, and support over the past few years. I will miss our many coffees together at Grad House.

Finally, thank you to my family and friends for your support. Taylor Maitland, Sam Ayers-Glassey, and Susan Wells, I wouldn't have made it without your encouragement.

Table of Contents

Author's Declaration ii

Abstract iii

Acknowledgements vi

List of Figures ix

List of Tables xii

List of Abbreviations xiii

Chapter 1: Introduction 1

1.1 General Background 1

1.2 Objectives 5

Chapter 2: Background 7

2.1 Activated Carbon for Permeable Reactive Barriers 7

2.1.1 Mechanisms of PFAS Adsorption 9

2.1.2 Adsorption Kinetics and Isotherms 11

2.1.3 Effect of solution chemistry on the adsorption of PFAS to CAC 13

2.2 Biofilms 16

2.2.1 Biofilm Growth and Development in Batch Systems 16

2.2.2 Biofilms in Activated Carbon Permeable Reactive Barriers for PFAS 18

Chapter 3: Materials and Methods 22

3.1 Materials 22

3.2 Experimental Methods 24

3.2.1 Preparation of *P.putida* Culture 24

3.2.2 Growth of *P.putida* Growth in the Absence of Particulates 24

3.2.3 Growth of *P.putida* in the Presence of CAC and Sand 27

3.2.4 Adsorption Experiments 28

3.2.5 Analytical Methods 32

3.2.6 Statistical Methods 37

Chapter 4: Results and Discussion 38

4.1 Characterization of *Pseudomonas Putida* 38

4.1.1 Growth 38

4.1.2 Attachment of Biofilm to Colloidal Particles 41

4.2 Impact of Biofilms on PFAS Adsorption 47

4.2.1 Effect of the concentration of broth on PFOS adsorption and biofilm formation 47

4.2.2 Adsorption Kinetics 52

4.2.3 Effect of biofilm on the adsorption of PFOS and PFPeA at different aqueous phase concentrations 57

Chapter 5: Conclusions and Recommendations 62

Citations 64

Appendix A: Artificial Groundwater Recipe A-1

Appendix B: Additional CLSM Images B-1

List of Figures

Figure 1-1: Chemical structure of (A) PFOS and (B) PFPeA..... 3

Figure 1-2: Schematic of an activated carbon permeable reactive barrier installed by injection through a direct push drill rig..... 4

Figure 3-1: Growth curve procedure for (A) 80 mg/L broth and (B) 3 mg/L Broth conditions .. 25

Figure 3-2: Experimental procedure for three-day adsorption experiments: bacterial control, 1-P, 2-P, 3P, and 4-P. 32

Figure 4-1: Growth of P.putida in 50 mL AGW containing 3 mg/L or 80 mg/L beef broth as indicated by A) Optical Density and B) pH. Vertical error bars represent one standard deviation of three replicate measurements. 40

Figure 4-2: CLSM maximum intensity projections of samples from microcosms incubated in the absence of bacteria. (A) Set 1 contained CAC and (B) Set 2 contained fine silica sand. The clumping of particles visibe in these images is an artifact of the dye process and therefore not representative of the bacteria-free particle distribution before dying. 42

Figure 4-3: Microcosm Set 3: P.Putida incubated in AGW with 80 mg/L broth in the absence of particulate. (A) Images observed under CLSM using only visible light and (B) Overlaying the visible light with a maximum intensity of the fluorescent dyes. 43

Figure 4-4: Images (A) and (B) show visible light projections of CLSM images of Set 4, bacteria-coated CAC (A) and Set 5, bacteria coated sand (B) incubated in the presence of P.putida and 80 mg/L broth in AGW. The particulate appears as dark grey or black. Images (C) and (D) show visible light projections overlayed with the maximum intensity of the fluorescent dyes for P.Putida-coated CAC (C) and Sand (D). Cells are coloured green and EPS is coloured red. 44

Figure 4-5: Samples from microcosm (A) Set 1, CAC in the absence of bacteria and (B) Set 4, CAC with P.putida collected after the incubation period in AGW with 80 mg/L broth. Samples were allowed to settle for 10 minutes before being photographed. 45

Figure 4-6: Thickness and roughness of biofilm on CAC during growth in a microcosm with 3 mg/L Broth as measured using CLSM. Vertical error bars represent one standard deviation. 47

Figure 4-7: The effect of added broth on the adsorption of PFOS to CAC. Reaction solutions contained 0.12 g/L CAC and a starting concentration of 0.26–2.5 mg/L of PFOS. Fitting lines represent (A) a linear model (B) a Freundlich model and (C) a Langmuir model of the data. Fitting parameters are listed Table 4-1. Error bars represent one standard deviation of replicate measurements. 48

Figure 4-8: Biofilm formation on CAC after seven days of incubation in AGW for experiments A) 3-P (1.2 mg/L broth) B) 2-P (3 mg/L) broth and C) 1-P (80 mg/L broth) 50

Figure 4-9: Variation in biomass thickness, and roughness of P.Putida biofilm grown in experiments 1-P, 2-P, and 3-P, after seven days. Each point represents the value of an individual image. Values for cells are shown in green, values for EPS are shown in Red. 51

Figure 4-10: PFAS adsorption on biofilm-free and biofilm-coated CAC over 5 to 8 days. Reaction solutions contained 0.12 g/L CAC, 3 mg/L broth, and 0.65 mg/L PFOS or 0.398 PFPeA. Error bars represent one standard deviation of replicate measurements. 54

Figure 4-11: Adsorption kinetics of PFOS sorption to bacteria-free and P.putida containing CAC wit with (A) a first order kinetic model and (B) a pseudo-second order kinetic model. Fit parameters are listed in Table 4-3. 55

Figure 4-12: Average thickness and roughness of cells and EPS measured during 5-day kinetic PFOS adsorption experiment. Reaction solutions contained 0.12 g/L CAC, 3 mg/L broth,

and 0.65 mg/L PFOS in AGW with 3 mg/L broth. Vertical error bars represent one standard deviation. 56

Figure 4-13: Biofilm formation on CAC particles after (A) 1 day, (B), 3 days, and (C) 5 days in contact with PFOS during the kinetic experiment. Reaction solutions contained 0.12 g/L CAC, 3 mg/L broth, and 0.65 mg/L PFOS in AGW with 3 mg/L broth. Additional images of the biofilm during the kinetic experiment are presented in Appendix B. 57

Figure 4-14: The effect of biofilm on the adsorption of PFOS to CAC. Reaction solutions contained 0.12 g/L CAC and starting concentrations of 0.26–2.5 mg/L of PFOS and (A) 80 mg/L broth and (B) 3 mg/L broth. 59

Figure 4-15: Distribution of PFPeA between aqueous phase and CAC after three days for biofilm-free and biofilm-coated CAC. Error bars represent one standard deviation..... 60

Figure 6-1: Images A and B a show visible light projections of CLSM images of bacteria coated sand. The Particulate appears as dark grey or black points and is to be embedded within the translucent grey cellular matrix. Images C and D show the visible light projections overlayed with the maximum intensity of the fluorescent dyes for P.Putida Sand. Cells are highlighted in green and EPS is coloured red..... B-1

Figure 6-2: Confocal images P.putida incubated in AGW containing 30µL of CAC and 3 mg/L of broth over seven days. As samples are not returned to microcosms after microscopy, the images show separate sections of biofilm from each day. Cells are highlighted in green and EPS is coloured red. B-2

Figure 6-3: P.putida biofilm assumed to be in the stationary phase of growth over the course of five day kinetic experiment. Days are indicated as days from the addition of PFOS, day 0 is when PFOS was added, day 1 is 24 hours later, etc. As samples are not returned to microcosms after microscopy, the images show separate sections of biofilm from each day. Cells are highlighted in green and EPS is coloured red. B-3

List of Tables

Table 2-1: Literature K_d values for PFAS adsorption to CAC.....12

Table 3-1: Composition of microcosms used to examine the biofilm formation on CAC and fine sand. 28

Table 3-2: Summary of 3 Day Multi-Point Adsorption Experiments.....31

Table 4-1: Parameters for a linear, Freundlich, and Langmuir model fit to the adsorption of PFOS on abiotic CAC in the presence of nutrient broth (Figure 4-7). Error presented is equal to the standard error of the value. 49

Table 4-2: Thickness and roughness of P.putida biofilm grown on CAC particles. Error represents the standard deviation of the values 50

Table 4-3: Kinetic coefficients for the adsorption of PFOS to bacteria-free and P.putida containing CAC (Figure 4-11) 55

Table 4-4: K_d values for bacteria free CAC, P.putida containing CAC, and P.putida in the absence of CAC as shown by linear data fit on Figure 4-14 and Figure 4-15 59

List of Abbreviations

AC	Activated Carbon
AFFF	Aqueous Film Forming Foams
AGW	Artificial Ground Water
CAC	Colloidal Activated Carbon
CLSM	Confocal Laser Scanning Microscopy
ConA	Concanavalin A dye
DOC	Dissolved Organic Carbon
EPS	Extracellular Polymeric Substance
GAC	Granular Activated Carbon
HDPE	High-Density Polyethylene
LC-MS/MS	Liquid Chromatography Tandem Mass Spectrometry
OD	Optical Density
PAC	Powdered Activated Carbon
PCB	Polychlorinated Biphenyls
PFAS	Per- and Polyfluoro Alkyl Substances
PFOA	Perfluorooctanoic Acid
PFOS	Perfluorooctanesulfonic Acid
PFPeA	Perfluoropentanoic Acid
pK_a	Acid Dissociation Constant
P.putida	*Pseudomonas putida*
PRB	Permeable Reactive Barrier
PZC	Point of Zero Charge

Chapter 1: Introduction

1.1 General Background

Per- and polyfluoroalkyl substances (PFAS) are a class of chemicals consisting of at least one carbon atom fully saturated with fluorine (C_nF_{2n+1}) (Buck et al., 2011; Evich et al., 2022). PFAS are thermally and chemically stable, and can repel oil and water (Buck et al., 2011; Glüge et al., 2020; Z. Wang et al., 2017). Owing to these properties, PFAS are used in products and applications such as chemical processing aids, textile surface protectants, paper packaging coatings, and firefighting foam surfactants (Glüge et al., 2020). PFAS were first produced in the 1940s, and it has been estimated that there may now be over 14,000 different chemicals that are being used in over 200 applications (Glüge et al., 2020).

With increased production and use, PFAS have also been more frequently detected in the environment. PFAS can be discharged via liquid waste streams or air emissions at industrial production facilities (Evich et al., 2022). Air emissions result in long-range transport of PFAS, affecting a large area. For example, one study estimated that 95% of the 109,000 kg of PFAS released in a year at an industrial facility were transported over 150 km (D'ambro et al., 2021). PFAS can also leach out of products during their use (McGarr et al., 2023; Nilsson et al., 2010). Additionally, PFAS could continue to leach out from products after they have been disposed of at landfills, resulting in the presence of PFAS in landfill leachate (Hu et al., 2016; Stoiber et al., 2020). Because landfill leachate is typically treated at a municipal wastewater treatment plant, it could be a significant contributor of PFAS to wastewater effluent and biosolids.

Due to the various pathways through which PFAS enter the environment, they have been detected globally in soil, surface water, and groundwater (Giesy & Kannan, 2001; Johnson et al., 2022).

PFAS also have been found in wildlife tissues and humans, due to exposure to contaminated soil and water (Brusseau et al., 2020; Giesy & Kannan, 2001; Johnson et al., 2022). Worldwide, humans have been exposed to PFAS as indicated by detectable concentrations in blood, urine, and breast milk (Jian et al., 2018). The presence of PFAS in wildlife and humans is a significant concern because toxicological studies have shown that PFAS exposure may result in changes in immune and thyroid function, insulin dysregulation, kidney disease, adverse reproductive and developmental outcomes, and cancer (Fenton et al., 2021; US EPA, 2016). While most individuals are only exposed to low-level concentrations of PFAS through diet, those living near a PFAS-contaminated site could face a substantially higher risk, with up to 75% of exposures coming from contaminated drinking water (De Silva et al., 2021; Hu et al., 2019; Vestergren & Cousins, 2009).

The sites most frequently associated with PFAS contaminated drinking water supplies are airports and military installations where PFAS-containing aqueous film-forming foams (AFFF) were used during firefighter training (Hu et al., 2016). In Canada, it is estimated that 420 airports may have been impacted by PFAS, while in the United States, as many as 664 military firefighting training areas and 533 civilian airports may have been impacted by PFAS from AFFF (Hu et al., 2016; Milley et al., 2018). Groundwater at AFFF-impacted sites may contain as many as 240 individual PFAS, in addition to co-contaminants such as petroleum hydrocarbons and chlorinated solvents (Barzen-Hanson et al., 2017; Carey et al., 2022). Perfluorooctane sulfonic acid (PFOS, Figure 1-1A) is one of the most commonly detected compounds at AFFF sites, but shorter-chain compounds, such as perfluoropentanoic acid (PFPeA, Figure 1-1B), could also be present. Compared to PFOS, PFPeA is more hydrophilic and mobile (Ateia et al., 2019; Carey et al., 2022; Minh et al., 2020).

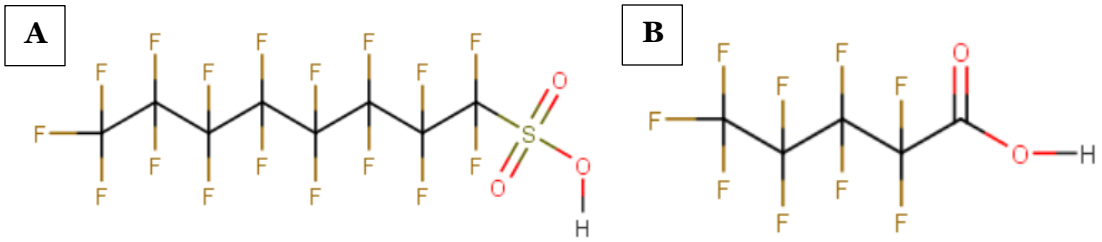


Figure 1-1: Chemical structure of (A) PFOS and (B) PFPeA

Once PFAS enter the environment, they are persistent because their carbon-fluorine bonds are resistant to most chemical and biological degradation. Although techniques such as advanced oxidation, plasma, high-temperature treatments and electrochemical oxidation have been shown to be promising for the destruction of PFAS (Gebregiorgis Ambaye et al., 2022), they must be applied ex-situ and can be energy intensive, making them difficult and costly to implement on a large scale. Currently, the most viable treatment method to remove PFAS from contaminated groundwater is "pump-and-treat", which involves pumping groundwater and subsequently treating the water by adsorption or membrane filtration (Abbasian Chaleshtari & Foudazi, 2022). While effective, pump-and-treat systems can be expensive to implement because of long operational times and the need for regular monitoring and maintenance.

Recently, it has been suggested that in-situ immobilization of PFAS using permeable reactive barriers (PRBs) could be a cost-effective method to manage the downgradient risk associated with a PFAS impacted site (McGregor, 2020b). A PRB consists of material placed perpendicular to the ambient groundwater flow direction to adsorb contaminants as they migrate through the barrier (Figure 1-2*)* (Obiri-Nyarko et al., 2014). Traditionally, PRB amendments were placed in a PRB by open cut trenching; however, injection methods have gained popularity as it does not require excavation and has the potential to reach greater depths (Gavaskar, 1999; Thiruvenkatachari et al., 2008). Compared to ex-situ remedial approaches, PRBs present an effective and low-cost method for the management of PFAS sites. Some estimates indicate total PRB costs may be only

a third of the cost of a pump-and-treat system (Birnstingl & Wilson, 2024; Sakr et al., 2023; Scherer et al., 2000)

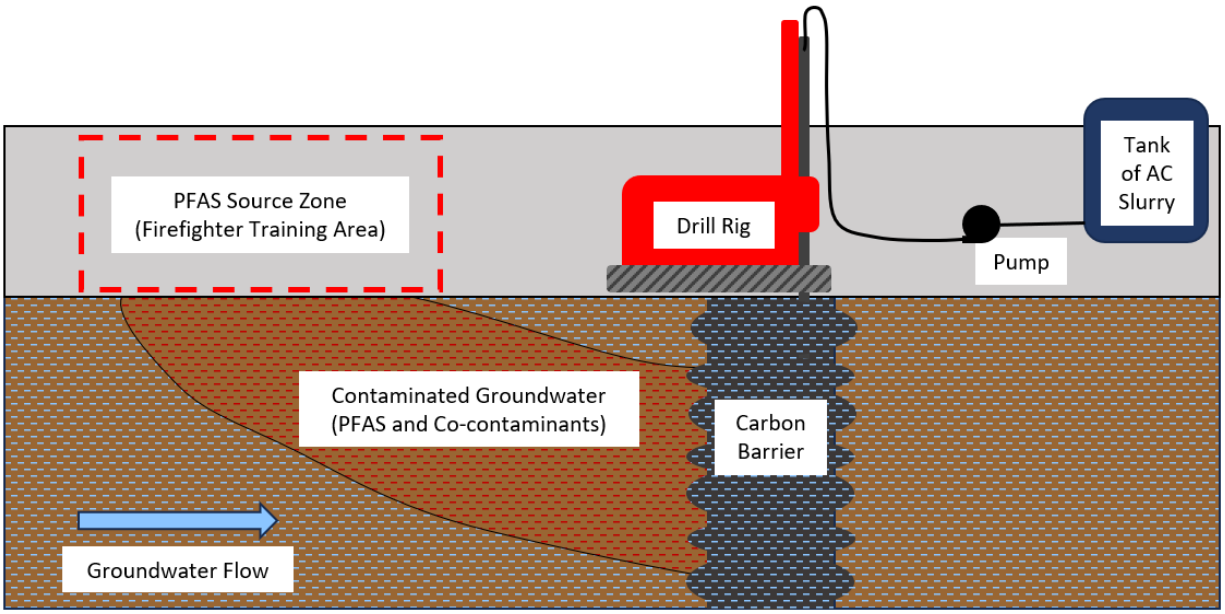


Figure 1-2: Schematic of an activated carbon permeable reactive barrier installed by injection through a direct push drill rig

Activated carbon (AC) is an effective adsorbent for a wide range of contaminants and has been deemed an effective amendment for use in PRBs designed to immobilize PFAS. Colloidal activated carbon (CAC; diameter of 1–2 µm) and powdered activated carbon (PAC; diameter of 25–100 µm) are commercially available injectable AC products, which have been used widely (Obiri-Nyarko et al., 2014). CAC is injected under lower pressures compared to PAC, and due to their polymer coating and smaller size are distributed more uniformly in the subsurface (McGregor, 2020). The ability of CAC to mitigate PFAS migration has been investigated in both laboratory and field experiments (McGregor, 2018, 2020b; Niarchos et al., 2022).

AC particles in a PRB adsorb contaminants and interact with the other aqueous subsurface components, including microbes. Over time, native microorganisms can form a biofilm on the AC surface and, in some cases, increase the overall microbial diversity (McGregor, 2020). Biofilm presence on AC can regenerate sorption sites by degrading organic matter as it desorbs from the carbon surface thereby limiting re-adsorption (Aktaş & Çeçen, 2007; Simpson, 2008). It is currently unclear the extent to which bioregeneration occurs within an AC PRB (Fan et al., 2017). For example, a study on the sorption of polychlorinated biphenyls (PCB) to granular activated carbon (grain size < 200 μm) indicated that biofilm-covered AC had an equilibrium sorption capacity that was an order of magnitude less than the virgin material (Mcdonough et al., 2007). In another study, Dalahmeh et al. (2019) observed a reduced adsorption of 3-9 perfluorinated carboxylic acids and C3, C6, and C8 perfluorinated alkyl sulfonates on biochar coated with biofilm. Both studies attributed the decrease in sorption to the blockage of sorption sites by biofilm. To date, no study appears to have evaluated the effect of biofilm presence on the adsorption of PFAS to AC. Also, given that CAC particles are similar to the size of a bacterial cell (1–2 μm), it is unclear if CAC particles can support biofilm formation (Fan et al., 2017).

1.2 Objectives

The objectives of this research are to (1) determine whether biofilm can be formed on CAC, and (2) to examine the effect that biofilm may have on the ability of CAC to adsorb PFAS. Results generated from this research will help improve our understanding of how biofilm may affect the adsorption of PFAS in CAC PRBs.

The objectives were investigated in three stages, characterization of bacterial growth in the absence of particulate, characterization of growth in the presence of particulate, and PFAS

adsorption experiments. By characterizing the growth of bacteria without particulate, the incubation period required for the bacteria to reach the stationary phase of growth under experimental conditions was found. This incubation time was then used to ensure a fully developed biofilm was present in subsequent experiments. Bacterial growth was then characterized in the presence of CAC or fine sand to address the first objective of this research. The second objective was then assessed using kinetic and three-day adsorption experiments. Results from these experiments indicated how biofilm may impact the adsorption rate and capacity CAC for PFAS compounds. Chapter 2 provides additional background information for this research, Chapter 3 describes the materials and research methods used, Chapter 4 presents the results obtained, and Chapter 5 summarizes the conclusions and recommendations resultant from this work.

Chapter 2: Background

2.1 Activated Carbon for Permeable Reactive Barriers

Activated carbon is a common material used to adsorb a wide variety of contaminants. Commercial activated carbon products can be manufactured from source materials such as coconut shells, wood, or coal by physical or chemical activation (Yahya et al., 2015). During physical activation, the source material is first carbonized by heating in the absence of oxygen to a temperature of 500°C to volatilize non-carbonaceous material, then is activated by heating the material to between 750°C and 950°C to increase the pore size and volume while oxidizing the surface to create active sites (Arena et al., 2016). In chemical activation, the source material is impregnated with a catalyst that dehydrates and degrades the cellulose. The material is then washed with an acid or base (depending on the specific catalyst used) to remove the chemical reagents and leave behind a high-porosity structure (Yahya et al., 2015). The final product of both manufacturing methods is a particulate formed from randomly oriented graphite sheets with an extremely high pore volume (0.7–1.8 cm^3/g) and surface area (500–1500 m^2/g) (Aktaş & Çeçen, 2007; US EPA, 2018). AC is set apart from similar carbon-based remediation products, such as biochar, because the activation process oxidizes the carbon and increases the number of micropores available for sorption (Çeçen &Aktaş, 2011). AC is used frequently to remove organic contaminants from water by adsorption.

PAC and CAC are typically used for in-situ remediation because they can be injected into the subsurface (US EPA, 2018). The smaller particle size of CAC (1–2 μm diameter) may provide advantages over courser grained PAC (25–100 μm diameter). Because CAC particles are smaller than the typical distance between soil grains, CAC can be injected at much lower pressure (30–50 psi), while PAC injection typically involves a high pressure (300–1000 psi) and some degree of hydraulic fracturing (Fan et al., 2017; US EPA, 2018). A field study of CAC and PAC application

also indicated that CAC was able to distribute more evenly in the aquifer, whereas PAC accumulated more in high hydraulic conductivity seams (McGregor, 2020). Assessing the utility of CAC for the remediation of groundwater contaminated with emerging contaminants, including PFAS, has been an active study area.

Plumestop™, a commercial CAC product developed by Regenesis, has been used in the remediation of hydrocarbons and chlorinated solvents (US EPA, 2018). This proprietary product includes CAC particles suspended in an aqueous solution containing polymers. The role of the polymers is to prevent the aggregation of CAC particles, thereby allowing the CAC particles to spread in the subsurface and create an adsorptive zone (Ndubueze et al., 2024). In one case study, the site-specific CAC distribution was measured to be 4.57 m from the injection point (McGregor, 2018). By closely spacing CAC injection points, a PRB can be emplaced to mitigate contaminant transport.

When PRBs are applied to PFAS, they have been shown to be a cost-effective option to immobilizes the fluorinated contaminants in groundwater (Birnstingl & Wilson, 2024). Three separate field trials of CAC injection saw a drop in PFAS concentrations. (McGregor, 2018; McGregor & Benevenuto, 2021; Niarchos et al., 2023). Niarchos et al. (2023) found that, after carbon injection, the total PFAS concentration was initially reduced by 76% but saw a rebound in concentrations after six months resulting in final reduction in total PFAS of 52%.. McGregor & Benevenuto (2021) observed no rebound of PFAS in a shallow sand aquifer but noted an increase in the concentration of short-chain PFAS in a deeper fractured dolostone aquifer(McGregor & Benevenuto, 2021). This increase was attributed to the competitive sorption of PFAS and a reduced distribution of CAC in the fractured rock compared to the sandy area. It is evident in all

studies that an understanding of both site characteristics and the underlying mechanism of adsorption is critical to designing and implementing CAC barriers.

2.1.1 Mechanisms of PFAS Adsorption

The adsorption of PFAS to AC occurs by two primary mechanisms, hydrophilic attachment of the ionic head group and hydrophobic interaction of the fluorocarbon tail (Abbasian Chaleshtari & Foudazi, 2022). Hydrophilic interactions are driven by the ionized PFAS head group being electrostatically attracted to the positively charged carbon surface (Abbasian Chaleshtari & Foudazi, 2022; Gilak Hakimabadi et al., 2023). Hydrophobic interactions are driven by the Van der Waals forces between the PFAS's fluorinated tail and the non-polar surfaces of AC (Du et al., 2014; van Oss et al., 1980). For longer-chain PFAS, it is generally agreed that hydrophobic interactions drive adsorption, particularly as the length of the C-F chain increases (Gilak Hakimabadi et al., 2023; Sorengard et al., 2019).

An additional type of hydrophobic interaction is the formation of micelles and hemi-micelles, where groups of PFAS molecules cluster with their hydrophobic tails pointed together and hydrophilic head groups exposed to the surrounding groundwater (Abbasian Chaleshtari & Foudazi, 2022). Even when the concentration of PFAS is lower than the critical concentration for micelle formation, it has been hypothesized that the higher localized concentrations of PFAS near the carbon surface or inside pores can allow for the formation of micelles or hemi-micelles that are attached to the surface. (Abbasian Chaleshtari & Foudazi, 2022; Q. Yu et al., 2009). As a result, the adsorption of PFAS could be enhanced by micelle formation.

Between different AC products, PFAS sorption is impacted by differences in the distribution of macropores (>0.05 μm), mesopores (0.002–0.05 μm), and micropores (<0.002 μm) (Carey et

al., 2022). CAC and PAC typically contain more micropores, while GACs typically contain more meso and macropores (Molé et al., 2024; Q. Yu et al., 2009). Because a molecule of PFOS is approximately 0.001 μm long (Erkoc & Erkoc, 2001), it is expected that longer-chain PFAS would predominantly Adsorb in larger mesopores, while short-chain compounds would be predominantly adsorbed in micropores (Du et al., 2014). Saeidi et al. demonstrated this correlation, finding that the adsorption capacity of PFOS and PFOA were related to the volume of pores between 0.001 and 0.002 μm but unrelated to the volume of pores smaller than 0.001 μm (Saeidi et al., 2020). A study performed by Molé et al. (2024) corroborated the effect of pore size on the adsorption of short-chain PFAS to CAC. In particular, Molé et al. (2024) reported that low molecular weight organic carbon that was able to block micropores had a larger impact on the sorption of short-chain PFAS than higher molecular weight compounds, which are primarily adsorbed in larger mesopores(Molé et al., 2024).

Despite the increase in surface area and pore volume associated with a smaller particle size, CAC has been shown to adsorb less PFAS than PAC of the same material due to the oxidation of the carbon surface during milling (Gilak Hakimabadi, 2024). However, the increased surface area of CAC is able to provide a kinetic advantage for sorption with equilibrium being reached within 6 hours for CAC as opposed to 48 hours for PAC (Gilak Hakimabadi, 2024). Additionally, the ability to inject CAC at lower pressures than PAC, and CAC's ability to disperse between sand grains in the subsurface provide practical advantages for the installation of PRBs and the distribution of the material in-situ. Therefore, the study of CAC for use in the management of PFAS in groundwater remains a worthwhile area of investigation.

2.1.2 Adsorption Kinetics and Isotherms

The adsorption of contaminants to AC can be characterized in terms of kinetics and isotherms, which describe the rate that a compound reaches equilibrium between the sorbed and the aqueous phases and the equilibrium distribution between the phases, respectively (Çeçen & Aktaş, 2011). By describing these processes mathematically, the information gained from batch adsorption experiments can more easily be compared and used in the modeling of contaminant transport in-situ (Worch, 2021)

The process of reaching adsorption equilibrium has been described as occurring through four steps, each of which can impact the overall kinetics. First, the compound must be transported through the aqueous phase to the boundary layer of water surrounding the sorbent. Transport of the compound can occur by diffusion or advection and is typically assumed to occur rapidly in a well-mixed system (Çeçen & Aktaş, 2011; Worch, 2021). Following bulk transport, the compound diffuses through the thin layer of water surrounding the sorbent particle, often referred to as external diffusion. Once reaching the surface, diffusion occurs through the pore spaces of the particle to available sorption sites (internal diffusion) (Worch, 2021).

Adsorption kinetics are frequently modeled using first-order kinetics as shown in equation 1 or pseudo-second order kinetics as shown by equation 2. In these equations C_s (mg/kg) is the sorbed concentration, k_1 (s^{-1}) is the first order rate constant, k_2 ($g \cdot mg^{-1} \cdot h^{-1}$) is the second order rate constant, C_{eq} (mg/L) is the aqueous concentration at equilibrium, and t (h) is time The kinetics of PFOS and PFOA adsorption onto AC have been found to be best fit by a pseudo-second order model (equation 2) equation 1, (Chen et al., 2017; Grieco et al., 2021; G. Kim et al., 2024).

$$C_s = C_{eq}\left(1 - e^{-k_1 t}\right) \quad (1)$$

$$C_s = \frac{k_2 {C_{eq}}^2 t}{1 + k_2 {C_{eq}}^2 t} \quad (2)$$

When describing contaminant adsorption to AC in terms of isotherms, the simplest case occurs when there is a linear relationship between the concentration adsorbed to the solid phase (C_s in mg/kg) and aqueous phase (C_{eq} in mg/L),.and the K_d value is the distribution coefficient (L/Kg) (equation 3). Linear isotherms are typically only applicable at very low concentrations or with natural sorbents such as minerals, which have weaker adsorption interactions than AC (Worch, 2021). However, the K_d remains a useful parameter for comparison between studies, and a linear fit has been found to well describe the sorption of PFOS to CAC (see Table 2-1)

$$C_s = K_d C_{eq}, \quad (3)$$

Table 2-1: Literature K_d values for PFAS adsorption to CAC

Compound	K_d (L/kg)	Experimental Setup	Study
Various PFAS	$10^3 - 10^5$	Column Experiments with CAC	(Niarchos et al., 2022)
PFOS	$10^{6.4}$	Batch Experiments with CAC	(Gilak Hakimabadi et al., 2023)
PFOS	$10^{2.5}$	Batch Experiments with CAC and Soil	(Sorengard et al., 2019)

The adsorption of compounds onto activated carbon is often better represented by the two-parameter isotherm models, i.e., the Langmuir or Freundlich isotherms. The Langmuir model assumes a monolayer of coverage of sorption sites which is represented by equation 4 (Çeçen & Aktaş, 2011), where $C_{s\,max}$ is the maximum sorbed concentration (mg/Kg) and K_L is the adsorption equilibrium constant (L/g). In contrast, the Freundlich isotherm, equation 5, does not assume that a monolayer of adsorbate is formed on the surface. In the Freundlich equation, K_f

$(mg/g)(mg/L)^{-n}$ is the Freundlich constant, while n is the exponential term that accounts for the heterogeneity of the AC surface (Worch, 2021). In general, the Freundlich model is commonly used when describing the adsorption of contaminants on AC (Jeirani et al., 2017).

$$C_s = \frac{C_{s_{max}} K_L C_w}{1 + K_L C_w} \quad (4)$$

$$C_s = K_f {C_w}^n, \quad (5)$$

2.1.3 Effect of solution chemistry on the adsorption of PFAS to CAC

The extent to which PFAS adsorb to CAC can be impacted not only by the CAC and PFAS properties but also by water chemistry parameters, including pH, ionic strength, and dissolved organic carbon (DOC) concentration. Under environmental pH conditions, the head group of many important PFAS compounds is negatively charged. These PFAS are either attracted to or repelled by AC, depending on the charge of the AC surface. The surface charge carried by a particle depends on the pH of the solution, with the surface being neutral when the pH equals the point of zero charge (PZC) of the material. When pH < PZC, the surface is positively charged and will exert an attractive force on anionic PFAS. Conversely, pH > PZC, the surface will be negatively charged and will repel anionic PFAS, resulting in a decrease adsorption (Saeidi et al., 2020). For PlumeStop™ CAC, Hakimbadi et al. found the PZC to be 11.8, while Ndubueze et al. found it to be 9.2 – 9.6 (Gilak Hakimabadi et al., 2023; Ndubueze et al., 2024). Differences in the estimates of PZC between studies have been attributed to differences in methods (Ndubueze et al., 2024). However, both PZC values suggest that the surface of PlumeStop CAC will be positively charged under neutral pH conditions. Thus, the adsorption of anionic PFAS on PlumeStop™ CAC will be driven in part by electrostatic attractions.

The impact of ionic strength on PFAS adsorption to AC has been depends on the surface charge of the sorbent, the chain length of the PFAS, and the concentration of ions present. Trends in of

increased or decreased sorption can be explained by the neutralization of surface charges, divalent cation bridging, and salting out effects.

The neutralization of surface charges occurs when the charged surface of the sorbent attracts a layer of oppositely charged ions in solution resulting in weakened electrostatic interactions between the carbon and intended contaminant (G. Kim et al., 2024). For a negatively charged sorbent, a high ionic strength solution can form a layer of positively charged ions that shield PFAS from electrostatic repulsion and thereby increase the extent of PFAS sorption (G. Kim et al., 2024). However, the surface of CAC is typically positively charged under environmental pH. Therefore, in high ionic strength solution, a layer of negatively charged ions is expected to form causing a reduction in electrostatic attraction and therefore decreased sorption of anionic PFAS (Umeh et al., 2023). In a comparison of the sorption of 14 PFAS compounds to PAC, Kim et al. (2024) observed that when the ionic strength was increased to 20mM the largest decrease in sorption occurred for short chain PFPeA and octafluoroadipic acid (compounds with 4 fully fluorinated carbons) while almost no change in sorption occurred for long chain PFOS or perfluorododecanoic acid (a compound with 11 fully fluorinated carbons)(G. Kim et al., 2024). It has been concluded that the effect of surface charge neutralization is most prevalent for short-chain PFAS because sorption is driven to a greater extent by electrostatic interactions, whereas long-chain compounds primarily interact with the carbon surface hydrophobically (Umeh et al., 2023).

In solutions in which the carbon surface is negatively charged, increased ionic strength can result in increasing sorption for long-chain PFAS through cation bridging (Du et al., 2014; G. Kim et al., 2024). Bridging occurs when divalent cations (Ca^{2+}, Mg^{2+}, or Cu^{2+}) form weak complexes between the negatively changed functional groups on the sorbent surface and anionic PFAS head groups

(Du et al., 2014; W. Wang et al., 2021). However, it remains unclear why cation bridging appears to occur predominately for long chain compounds over short chain (Cai et al., 2022).

The salting out effect can also increase the sorption of long chain PFAS in high ionic strength solution. Salting out occurs when the high ionic strength causes PFAS to become less soluble in the aqueous solution (Du et al., 2014). As a result of decreased solubility, PFAS are increasingly deposited onto aquifer solids and sorbed to available adsorbent surfaces (Du et al., 2014; Hort et al., 2024)Salting out is typically studied in the context of marine systems where the deposition of PFOS onto aquifer solids can increase between four and fifteen times between freshwater and saltwater systems Click or tap here to enter text. (Hort et al., 2024).

In addition to impacts from ionic strength, a significant reduction in PFAS sorption can also occur due to DOC in solution. The effect DOC has been observed for both CAC and PAC products and the decrease in sorption is typically attributed to competition for available sorption sites (Gilak Hakimabadi et al., 2023; Molé et al., 2024; J. Yu et al., 2012). Contrary to the common assertion that DOM inhibits sorption by blocking pores meso- and micropores, further evaluation has shown that inhibition is more likely caused by competition between PFAS and DOM for sorption sites on the carbon surface (Gilak Hakimabadi et al., 2023; J. Yu et al., 2012). Competitive sorption was determined to be the more likely cause as a comparison of different sized DOM constituents showed the greatest inhibition to sorption by compounds with lower molecular weights, more similar to the size of PFAS (J. Yu et al., 2012). It is of concern that in the presence of biofilm, the amount of small DOM molecules generated will decrease the observed extent of PFAS removal.

2.2 Biofilms

Microorganisms are ubiquitous in the subsurface and often form complex, surface-attached communities called biofilms (O'Toole et al., 2000). A biofilm is held together by extracellular polymeric substances (EPS), which are secreted by the bacterial cells and allow the biofilm to form larger connected structures (Flemming & Wingender, 2010; Zhang & Fang, 2001). The composition of the EPS can vary based on environmental factors but typically includes a variety of polysaccharides, proteins, DNA, lipids, and humic substances (Flemming & Wingender, 2010; Schlafer & Meyer, 2017; Zhang & Fang, 2001). The constituents of the EPS hold bacteria much closer together than in the planktonic state, increasing stability, protecting against changes in environmental conditions, and allowing for sequestration of nutrients and enzymes (Flemming & Wingender, 2010; Probandt et al., 2017).

2.2.1 Biofilm Growth and Development in Batch Systems

Bacterial development in a batch system typically occurs in three distinct phases, lag, exponential, and stationary. During the lag phase, growth is limited as the cells adjust to the medium. Upon entering the exponential phase, growth increases rapidly as bacteria quickly multiply. Finally, during the stationary phase, the growth rate slows and becomes approximately equal to the rate of cell loss as nutrients become limited and waste products accumulate (Allen & Waclaw, 2018).

Biofilm development, which occurs during the exponential and stationary growth phases, is divided into five steps: reversable attachment, irreversible attachment, early development, maturation, and dispersion (Stoodley et al., 2002). The first step of biofilm development involves cells from the bulk fluid reversibly attaching to the surface by electrostatic attraction. Most bacteria are negatively charged and easily attracted to positively charged surfaces; however, even when the surface is negatively charged some bacteria are able to overcome the electrostatic

repulsion and attach using extracellular organelles such as flagella (Renner & Weibel, 2011). In both cases, bacterial attachment is further stabilized by van der Waals forces as hydrophobic functional groups on the cell wall are aligned with hydrophobic groups on the surface (Renner & Weibel, 2011).

Once single bacterial cells attach to the surface, the second step of biofilm development takes place as cells aggregate and begin producing EPS (Stoodley et al., 2002). There are three mechanisms by which aggregation occurs: movement of cells along the surface, cell division, or recruitment of cells from the bulk fluid (Stoodley et al., 2002). As cells aggregate, the production of EPS cements the cells together and to the surface. EPS can form up to 90% of the biofilm's final mass, and its role extends well beyond simply acting as a glue (Flemming & Wingender, 2010). The EPS protects the colony from mechanical stress and detachment, retains enzymes which promote nutrient availability, and holds DNA, which is then available for horizontal gene transfer (Flemming & Wingender, 2010; Renner & Weibel, 2011). Polysaccharides and proteins are primary EPS components, but the precise composition varies between biofilms and is dependent on microbial composition and environmental factors such as shear stress and temperature (Flemming & Wingender, 2010).

In the third and fourth steps of development, the biofilm uses cell-to-cell signaling known as quorum sensing to coordinate gene expression to form channels, pores, and other structures (Shrout et al., 2011). In one species of bacteria (*P.putida*), biofilm maturation was observed to consist of the bacteria's flagella reorganizing the cells into looser and more irregular structures that are thought to allow the biofilm to more efficiently utilize nutrients (Gjermansen et al., 2005; Tolker-Nielsen et al., 2000).

In the final step of biofilm development, cells are released from the biofilm to the bulk fluid (Renner & Weibel, 2011). While the dispersion of cells is typically described as the final stage, it has been shown to be more of a continuous process in which cells are continually released, which starts soon after a surface is first colonized (Bester et al., 2009). However, a full dissolution of the biofilm can also be triggered by environmental stressors, such as decreases in available nutrients (Gjermansen et al., 2005).

The study of biofilm development is typically associated with surfaces much larger than individual bacterial cells, such as glass flow cells (Bester et al., 2009) microtiter plates(Turonova et al., 2016) sand particles (Fu et al., 2023) or granular activated carbon (Aktaş & Çeçen, 2007). Rocha Díaz De León (2021) examined biofilm formation on PAC particles, which are smaller than sand or granular activated carbon but remain 25 to 100 times the size of an individual cell. A technical bulletin published by Regenesis (the manufacturer of Plumestop CAC) indicates that biofilm can form on CAC once it has attached to a larger sand particle. However, this conclusion was based on the correlation between biodegradation of hydrocarbon contaminants and increasing number of bacteria(Regenesis, 2023). Regenisis' investigation also assumed that biofilm would form only after CAC particles adhered to larger sand particles thereby providing a much larger surface for bacterial colonization (Regenesis, 2023). To date, no investigation of biofilm formation on CAC sized particles has been conducted.

2.2.2 Biofilms in Activated Carbon Permeable Reactive Barriers for PFAS

While PFAS compounds themselves cannot be biodegraded, biofilms may still impact the function of CAC PRBs. Possible impacts include: the sorption of PFAS to bacterial cells and EPS to slow contaminant transport, the degradation of non-PFAS compounds within the barrier to regenerate

sorption sites on the carbon surface, and the blockage of sorption sites by bacteria to reduce the adsorption capacity of CAC.

The sorption of PFAS to bacterial cells has been investigated as a possible mechanism for immobilization of PFAS (Butzen et al., 2020). In studies of PFOS and PFOA, the sorption of PFAS to planktonic bacterial cells is a rapid and reversable surface phenomena with no internalization of the contamination by the bacteria (Butzen et al., 2020; Dai et al., 2023). The extent of sorption is dependent on the PFAS chain length and head group with long chain compounds adsorbing more strongly than short chain, and sulfonic head groups more strongly than carboxylic acids (Butzen et al., 2020; Dai et al., 2023; Fitzgerald et al., 2018). The influence of cell wall structure has also been studied but is not conclusive. Buntzen et al. (2020) observed greater sorption of PFAS to gram-positive bacteria over gram-negative while Fitzgerald et al (2018) noted the opposite, and Dai et al. (2023) reported no difference in adsorption capacity between the bacterium types.

The sorption of PFAS to EPS has been shown to result in moderate reduction in contaminant transport (Dai et al., 2023). The effect of EPS appears to be greater than the effect of cells because of the EPS's protein-rich composition that enhances hydrophobic interactions. In two column studies using quartz sand (0.3–0.4 mm and 0.25–0.35 mm), PFAS retardation was observed to be proportional to the biomass present (Dai et al., 2023; Fu et al., 2023). By comparing PFOA retardation and the composition of three different species of biofilm, Fu et al. determined that PFOA migration was hindered most significantly by the biofilm with high, protein-rich EPS (Fu et al., 2023). This observation is consistent with other studies linking sorption to the proteins found in EPS (Kumar Pramanik et al., 2016; Yan et al., 2021). The ability of biofilm to slow PFAS transport may be of benefit to contaminated sites but has not been investigated on a larger scale.

Biofilms may also benefit CAC barriers by degrading non-PFAS compounds, such as co-contaminants or adsorbed organic matter, that may otherwise compete with PFAS for available sorption sites. While PFAS themselves cannot biodegrade, co-contaminants such as petroleum hydrocarbons and chlorinated solvents can be converted to innocuous byproducts by bacteria mediated oxidation or reduction reactions (Scherer et al., 2000). The presence of PFAS may cause soil bacteria to upregulate stress genes and increase biofilm formation but does not appear to influence the degradation of a co-contaminant such as toluene (Weathers et al., 2015). The injection of AC can further enhance biodegradation by promoting direct transfer of electrons between microorganisms and increasing bacterial diversity (Bonaglia et al., 2020; Simpson, 2008). In a field trial in which CAC was injected to immobilize PFOA and PFOS, it was observed that microbial diversity of bacteria and archaea was greater within the treated area than a control location located outside the plume after 18 months (McGregor, 2018). The removal of co-contaminants within a PRB is advantageous for the management of complex PFAS contaminated sites.

Dissolved organic matter has also been shown to decrease CAC's adsorption capacity for PFAS by occupying available sorption sites (Gilak Hakimabadi et al., 2023). Bioregeneration refers to a biofilm's ability to degrade this organic matter, thereby freeing up sorption sites for PFAS, which may be able to extend the life of an activated carbon (Aktaş & Çeçen, 2007). Bacteria are believed to bioregenerate the surface of activated by two mechanisms, the metabolism of accessible organic matter that has desorbed from the carbon surface and the excretion of enzymes that can diffuse into the pore space to reach and break down degradable components (Aktaş & Çeçen, 2007; Scholz & Martin, 1997). The effect of bioregenration was observed in a study by Dalahmeh et al. as the PFAS adsorption capacity of a biofilm coated biochar (1-5 mm diameter) was greater with a living

biofilm than an inactivated one. The decrease in adsorption capacity was attributed to the ability of an active biofilm to clear natural organic matter from the carbon surface resulting in a greater availability of sorption sites (Dalahmeh et al., 2019).

The effect of biofilm development on the sorption capacity of CAC for PFAS remains to be investigated. A study of the effect of biofilm on course-grained biochar (1-5 mm) on PFAS sorption observed a reduced capacity of the AC compared to virgin material (Dalahmeh et al., 2019; Scherer et al., 2000). A similar result was seen by Mcdonough et al. (2007) for the sorption of PCBs, a recalcitrant chlorinated compound, to biofilm coated and dissolved organic matter coated PAC. The biofilm and DOC coated PAC's adsorption capacity an order of magnitude lower than virgin material. The decrease in sorption capacity was attributed to the biofilm and dissolved organic matter adsorbing to or blocking sorption sites (Mcdonough et al., 2007). However, similar studies have not been conducted for colloidal carbon with PFAS. It remains unclear if biofilm is able to form on colloidal sized particles and what impact that may have on the sorption of PFAS to CAC.

Chapter 3: Materials and Methods

Bench-scale experiments were conducted to monitor the growth of planktonic bacteria, observe biofilm formation on particles <5 μm in size, and investigate the impact of biofilm on PFAS adsorption to CAC. Although natural biofilms are an amalgamation of different species, a single strain of bacteria was chosen for these experiments to reduce variability among replicates. *P.putida* was selected because it has been shown to readily form biofilms, is not infectious to humans, is commonly found in the environment, and has applications in the bioremediation of organic contaminants (Kivisaar, 2020). To inform the incubation time required in subsequent experiments, growth curves were generated for *P.putida*. The ability of the bacteria to form a biofilm on colloidal particles was then investigated by comparing bacteria incubated in the presence of CAC or fine sand with the bacteria incubated in the absence of a particulate. Subsequently, adsorption experiments were conducted with PFOS and PFPeA, which are among the PFAS commonly found at AFFF-impacted sites. With a long and fully fluorinated carbon chain, PFOS adsorbs to CAC predominantly through hydrophobic interactions, whereas PFPeA is a shorter-chain PFAS that is more hydrophilic and has a lower sorption affinity to CAC. Sorption experiments conducted with these two compounds provide an opportunity to observe the differences in sorption to CAC in the presence of a biofilm-forming bacteria.

3.1 Materials

The adsorbent used in this study was Plumestop™ (Regenesis, San Clemente, California, USA), which is a slurry containing 20 wt. % of CAC (1–2 μm particle diameter) in water. Plumestop also contains proprietary organic polymers whose role is to prevent CAC aggregation, thereby improving particle mobility in the subsurface. For comparison of the growth of *P.putida* on CAC to the growth on other particulates, fine silica sand (< 0.25 mm sieve) was used in some experiments.

Primary stocks of PFOS and PFPeA were purchased from Sigma Aldrich for use in sorption experiments. The PFOS stock contained 40% PFOS in water, while the PFPeA stock contained liquid PFPeA (97%, Sigma Aldrich, Darmstadt, Germany). From the primary stocks, two single-compound working stock solutions were prepared for each compound by dissolving aliquots of the primary stocks in LCMS grade methanol (Fisher Scientific, Waltham, Massachusetts). The concentration of PFOS or PFPeA in the working stocks was either 1,300 μM or 52,000 μM, which is equivalent to 650 mg/L or 2,600 mg/L for PFOS, and 343 mg/L or 1,373 mg/L for PFPeA. Native and isotopically labelled PFAS standards were purchased from Wellington Laboratories (Guelph, Canada). These standards were used to prepare calibration solutions and internal standards for LC-MS/MS analysis. For CSLM imaging work, fluorescent dyes Alexa Fluor® 633 Concanavalin A Conjugate and SYTO® 9 Green-Fluorescent Nucleic Acid Stain were purchased from Fisher Scientific, Waltham, Massachusetts.

The *P.putida* strain *Pseudomonas putida* (Trevisan) Migula (ATCC 12633) was purchased as a freeze-dried pellet from Cedarlane Labs (Burlington, Ontario). For bacterial culture growth and maintenance, powdered BD Difco™ Nutrient Broth BD 234000 was purchased from Fisher Scientific. The broth media is composed of 38 wt. % beef extract and 62 wt. % peptone but, as a complex media, the precise chemical composition is unknown. A broth solution was prepared by dissolving 2 g of powdered broth in 250 mL of Milli-Q water. As per the instruction from the supplier, the broth solution was then transferred to a 500 mL beaker and boiled for 1 min before being placed in a loosely capped 1 L bottle and autoclaved. For the growth and adsorption experiments, artificial groundwater (AGW) was prepared with sodium acetate (CH_3COONa, Fisher Scientific Waltham, Massachusetts) as a carbon source. See Appendix A for additional information about the composition of AGW and how it was prepared.

3.2 Experimental Methods

3.2.1 Preparation of *P.putida* Culture

The pellet of freeze-dried *P.putida* was rehydrated and grown in the broth solution following the procedure provided by the supplier (ATCC, 2022). Subsequently, the rehydrated *P.putida* was split into 0.6 mL aliquots. To each aliquot, 0.4 mL of a 50 v.% glycerol/Milli-Q water solution was added, and the resulting cultures (~ 1 mL/each) were stored in 2 mL centrifuge tubes at -80°C (Labauve & Wargo, 2012).

When handling the microbial culture, all surfaces, labware, and non-volatile chemicals were sterilized by autoclaving at 121°C or spraying with a solution of 70 v.% ethanol in water (Greenfield Global Inc., Toronto, Canada). The culture was handled in the sterile area surrounding the flame of a propane torch.

3.2.2 Growth of *P.putida* Growth in the Absence of Particulates

Experiments were conducted to monitor the growth of *P.putida* and determine the timing of the lag, exponential, and stationary phases of growth in the absence of a particulate. Experimental solutions contained an initial broth concentration of 80 mg/L or 3 mg/L, which represented systems containing high and low dissolved organic carbon (DOC) concentrations, respectively. Previous studies have shown that the adsorption of PFAS on CAC was diminished in the presence of DOC, presumably due to competitive sorption effects (Gilak Hakimabadi et al., 2023; Molé et al., 2024). Thus, experiments with high and low initial broth concentrations were conducted to observe the effect of the broth concentration on the growth of *P.putida* and, in adsorption experiments (described subsequently in section 3.2.3), of broth and biofilm on PFOS and PFPeA adsorption on CAC.

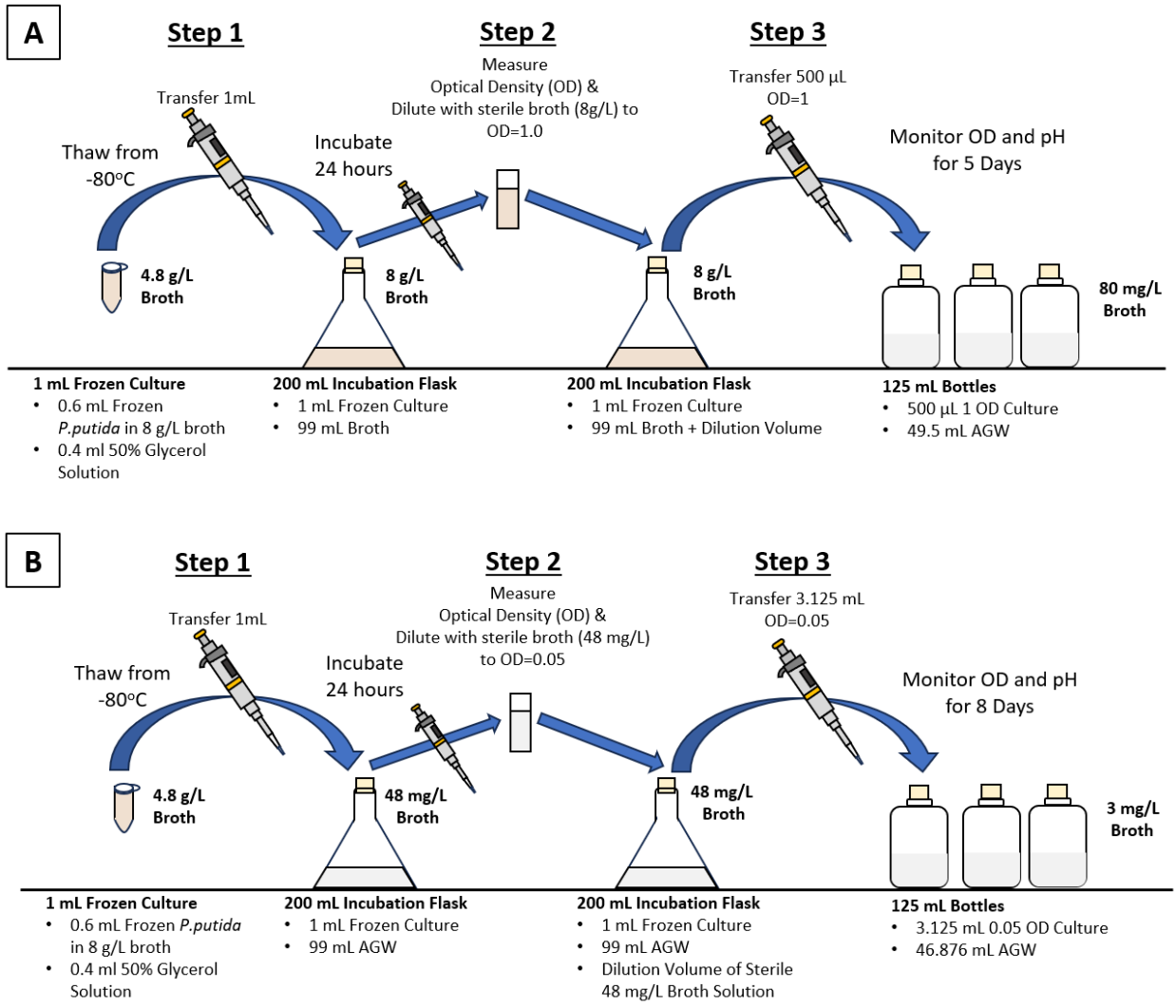


Figure 3-1: Growth curve procedure for (A) 80 mg/L broth and (B) 3 mg/L Broth conditions

Two different experimental procedures were employed to allow the broth concentration to be diluted while ensuring enough active bacteria were transferred at each step (Figure 3-1). In Procedure A, a 1-mL frozen aliquot of the *P.putida* culture was thawed and transferred to a 200 mL conical flask containing 99 mL of 8 g/L broth (Step 1). The flask was capped with a porous foam stopper (which allows ambient air to enter), placed on a shaker table, and incubated at room temperature. The OD of the solution was measured to confirm that the bacteria were growing (i.e., the *P.putida* culture had not been damaged during freezing and storage). After 24 hours of incubation, the OD of the solution typically ranged between 1.0 and 1.3. This solution was then

diluted to an OD of 1.0 using a solution containing 8 g/L of broth in water (Step 2), and 0.5 mL of the diluted solution was added to a 125 mL HDPE bottle (VWR International, Radnor, Pennsylvania) containing 49.5 mL of AGW (Step 3). Thus, Procedure A resulted in a 50 mL reaction solution with an initial broth concentration of 80 mg/L. Three HDPE bottles were constructed for each experiment. Because the reaction solution was constructed following the same procedure, it was expected that the initial cell concentration in all bottles would be similar. The HDPE bottles were capped with foam stoppers, placed on a rotary shaker, and incubated at room temperature for five days. During this period, the solution pH and OD were measured twice daily. The OD of a solution is proportional to the mass of cells present (Sutton, 2011), and thus the change in solution OD over time was attributable to the change due to bacterial growth.

Procedure B was used to generate growth curves for *P.putida* in a solution containing 3 mg/L of broth. The main difference between Procedure A and Procedure B was that in Step 1, the *P.putida* culture was grown in AGW instead of in the 8 g/L broth solution in order to dilute the concentration of broth in the culture to 48 mg/L. To this end, a 1-mL frozen aliquot of the *P.putida* culture was thawed and transferred to a conical flask containing 99 mL of AGW. The flask was then capped with a foam stopper, placed on a shaker table, and incubated for 24 hours. At the end of this period, the OD of the solution typically ranged between 0.06 and 0.08. In Step 2, the OD of the solution was diluted with an AGW solution containing 48 mg/L of broth to an OD of 0.05. In Step 3, 3.125 mL of the diluted culture was transferred to a 125 mL HDPE bottle containing 46.875 mL of AGW. A larger volume of inoculum was required in Procedure B (3.125 mL) than in Procedure A (0.5 mL) to allow enough bacterial cells transferred. As in Procedure A, the total volume of reaction solution in each bottle was 50 mL. The bottles were capped with a foam stopper and incubated on a rotary shaker for eight days. During this period, the solution pH and OD were measured twice daily.

All growth experiments were conducted in triplicate at room temperature. During analysis of results, OD values that were more than double the OD at previous and subsequent time points in a single microcosm were deemed to be outliers and were discarded.

3.2.3 Growth of *P.putida* in the Presence of CAC and Sand

Experiments were conducted to generate growth curves for *P.putida* in the presence of CAC and to determine if *P.putida* could form biofilm in the presence of colloidal particles. The growth of *P.putida* was investigated in solutions containing either 80 mg/L broth or 3 mg/L broth using the experimental procedures described in Section 3.2.2, with the following modifications. First, in Step 3, 0.03 mL of the CAC slurry was added to a 125 mL HDPE bottle containing either 47.47 mL (in Procedure A) or 46.845 mL (in Procedure B) AGW. Accounting for the volume of the added inoculum, the total reaction solution volume in each HDPE bottle was 50 mL, resulting in a CAC concentration of 0.119 g/L. Second, since CAC particles in the solution scattered light, the OD of the solution was not proportional to bacterial mass and thus could not be used to construct a growth curve. Therefore, the bacterial growth was deduced from the solution pH profile.

The following sets of samples were generated for CLSM imaging: 1) samples containing only CAC; 2) samples containing only sand; 3) samples containing *P.putida* grown in the absence of a particulate; 4) samples containing *P.putida* grown in the presence of CAC; and 5) samples containing *P.putida* grown in the presence of silica sand. Set 1 and 2 samples were used to evaluate the autofluorescence of CAC and sand. Set 4 samples were used to determine if *P.putida* was able to form a biofilm on particles <5 μm in size, while Set 5 samples were used to compare *P.putida* grown in the presence of CAC versus in silica sand, i.e., a larger-size particulate. CLMS images of Set 4 and 5 samples were also compared with the images of Set 3 samples. The composition of the reaction solutions used to generate these sample sets is presented in Table 3-1.

Table 3-1: Composition of microcosms used to examine the biofilm formation on CAC and fine sand.

Set #	Purpose	Particulate	*P.putida* Inoculum	AGW Volume	Total Microcosm Volume
1	Examine autofluorescence of CAC	0.03 mL CAC	None	49.97 mL	50 mL
2	Examine autofluorescence of Sand	Fine Silica Sand	None	50 mL	50 mL
3	Examine P.putida growth without particulate	None	0.5 mL	49.5 mL	50 mL
4	Examine P.putida growth in the presence of CAC	30 µL CAC	0.5 mL	49.47 mL	50 mL
5	Examine P.putida growth in the presence of sand	Fine Silica Sand	0.5 mL	49.5 mL	50 mL

An additional experiment was conducted to quantitatively assess the growth of *P.putida* in the presence of CAC. For this experiment, Procedure B was used to construct seven sets of triplicate microcosms, each containing 3.125 mL OD *P.putida* inoculum (OD = 0.05), 0.03 mL of CAC, and 46.845 mL of AGW. Microcosms were placed on a shaker table and incubated at room temperature. One set of triplicate microcosms was sacrificed each day for CLSM imaging. The CLSM images were used to calculate and compare the thickness and roughness of the bacterial cells and EPS.

3.2.4 Adsorption Experiments

Effect of broth on the adsorption of PFOS by CAC. As mentioned previously, DOC has been shown to suppress PFAS adsorption on CAC (Gilak Hakimabadi et al., 2023; Molé et al., 2024). Therefore, a preliminary experiment was conducted to evaluate the adsorption of PFOS on CAC in the presence of 0–80 mg/L broth. To this end, bacteria-free microcosms were prepared by adding either 0.5 mL of 8 g/L broth to 49.42 mL of AGW (thus, the initial concentration of broth was 80 mg/L) or a mixture of 0.6 mL of 8 mg/L broth and 0.4 mL of 50% glycerol to 99 mL of AGW (resulting in a broth concentration of 48 mg/L) then transferring 3.125 mL to 46.795 mL

of AGW, resulting in a broth concentration of 3 mg/L. The chemical composition of the broth aliquot transferred was similar to the chemical composition of the inoculums added in the experiments with *P.putida* (described below). After 0.03 mL of the CAC slurry was added, the bottles were incubated for three days. Subsequently, PFOS was added, and the bottles were incubated for three more days and were then subsampled for PFOS analysis.

Kinetics of PFOS and PFPeA adsorption by CAC in the absence or presence of P.putida. Following the investigation of the effect of broth on PFOS adsorption, experiments were conducted to determine PFOS and PFPeA adsorption kinetics on CAC in the presence of *P.putida*. These experiments consisted of two stages. In the first stage, *P.putida* was grown in the presence of CAC until the growth reached the stationary phase as determined in the previous phase of the research. PFOS or PFPeA was then added to the solution to initiate the second stage, i.e., adsorption. By allowing *P.putida* to reach the stationary phase prior to PFOS/PFPeA addition, changes in the biofilm thickness would be minimized during the adsorption phase.

For each experiment, fifteen microcosms were prepared. The bacteria-containing microcosms were constructed by adding 3.125 mL of *P.putida* culture (OD = 0.05) and 0.03 mL of a CAC slurry to a 125 mL HDPE bottle that contained 46.795 mL of AGW. The bottles were then incubated for four days, after which period PFOS or PFPeA was added to obtain an initial concentration of 0.65 mg/L PFOS or 0.343 mg/L PFPeA. The bottles were then incubated for another five days. During this period, three bottles were sacrificed each day and were subsampled for PFAS analysis and CLMS imaging.

For comparison, the kinetics of PFOS and PFPeA adsorption on CAC in the absence of *P.putida* was investigated. Fifteen bacteria-free microcosms were constructed by adding either 0.5 mL of

8 g/L broth to 49.42 mL of AGW or a mixture of 0.6 mL of 8 mg/L broth and 0.4 mL of 50% glycerol to 99 mL of AGW (resulting in a broth concentration of 48 mg/L), then transferring 3.125 mL to 46.795 mL of AGW, resulting in a broth concentration of 3 mg/L.

Adsorption in microcosms containing different initial concentrations of PFOS or PFPeA. Once the kinetics of PFOS and PFPeA adsorption on CAC had been established, the adsorption of these compounds at their different initial concentrations was further assessed. Bacteria-containing microcosms were constructed using the procedure described previously. In brief, *P.putida* inoculums were prepared (Steps 1 and 2) and then added to a 125 mL HDPE bottle that also received 0.03 mL of CAC (except in the Bacterial Control experiment) and 49.42 or 48.67 mL AGW (Step 3). The total volume of the reaction solution in each bottle was 49.95 mL. Subsequently, the bottles were capped with a foam stopper and incubated at room temperature. After four days, between 20 and 50 µL of a stock solution of either PFOS or PFPeA was added to the bottle to obtain six initial concentration levels of PFOS or PFPeA, ranging 0.5–5 µM (i.e., 0.26–2.5 mg/L of PFOS or 0.14 –1.4 mg/L of PFPeA). The initial concentrations in the experiment represent the PFAS concentrations in the groundwater at some AFFF-impacted sites. All bottles were then incubated for three more days and were then subsampled for PFAS analysis and CLSM imaging. Table 3-2 summarizes the three-day adsorption experiments conducted, while Figure 3-2 summarizes the experimental steps.

Table 3-2: Summary of 3 Day Multi-Point Adsorption Experiments

Identifier	PFAS	Initial Broth Concentration	Inoculum	Particulate	Replication
Null Control	PFOS	0 mg/L	None	CAC	1 Experiment in Duplicate
Bacterial Control		80 mg/L	*P.putida*	None	1 Experiment in Duplicate
1-A		80 mg/L	No *P.putida*	CAC	2 Experiments in Duplicate
1-P			*P.putida*	CAC	2 Experiments in Duplicate
2-A		3 mg/L	No *P.putida*	CAC	1 Experiment in Duplicate and 1 Experiment in Triplicate
2-P			*P.putida*	CAC	1 Experiment in Duplicate and 1 Experiment in Triplicate
3-A		1.2 mg/L	No *P.putida*	CAC	1 Experiment in Duplicate
3-P			*P.putida*	CAC	1 Experiment in Duplicate
4-A	PFPeA	3 mg/L	No *P.putida*	CAC	1 Experiment in Triplicate
4-P			*P.putida*	CAC	1 Experiment in Triplicate

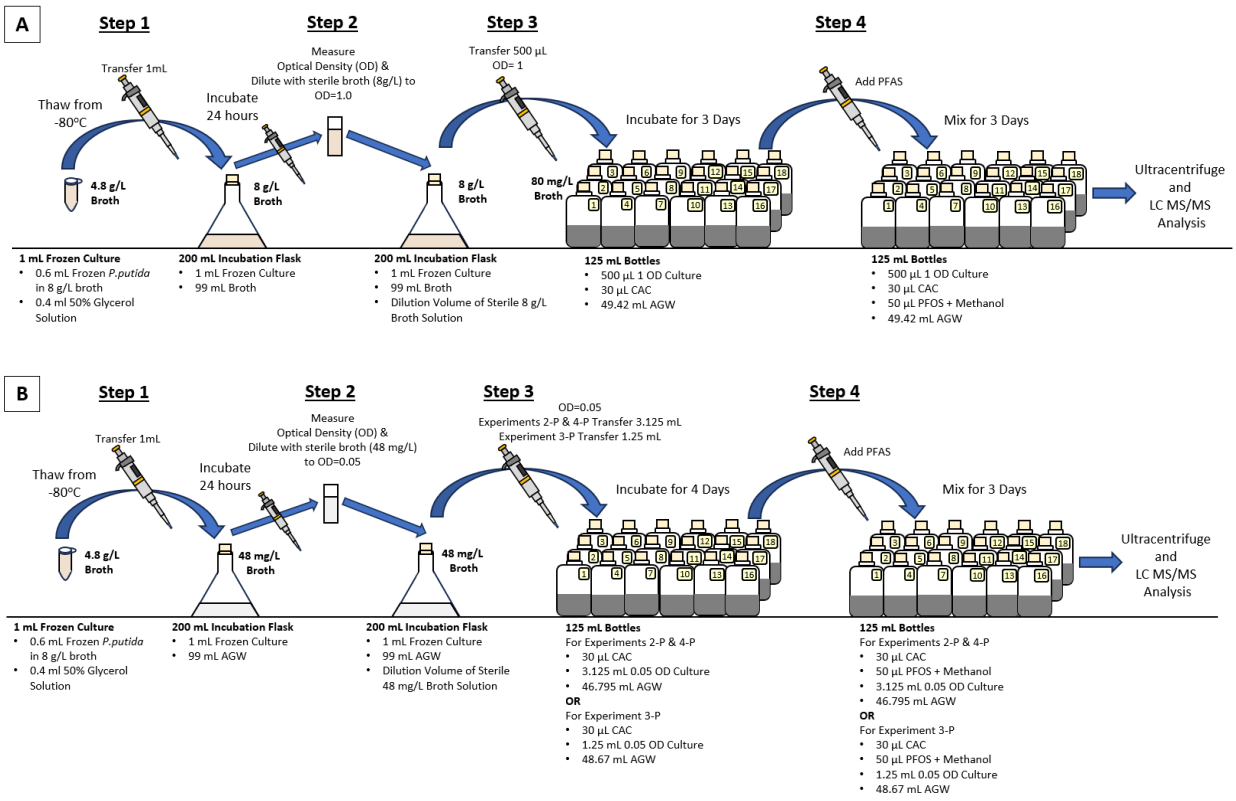


Figure 3-2: Experimental procedure for three-day adsorption experiments: bacterial control, 1-P, 2-P, 3P, and 4-P.

3.2.5 Analytical Methods

pH and Optical Density

Solution pH was measured using a Thermo Scientific Orion Star A329 multiparameter meter equipped with an Oakton pH probe. Optical density was used to monitor bacterial growth (Sutton, 2011). Samples were placed in cuvettes and allowed to settle for one minute before placing on a Thermos Scientific GENESYS 10S Series UV-Visible Spectrophotometer and analyzing for OD using l = 600 nm (Koch, 1970).

Microscopy – CLSM

Confocal Laser Scanning Microscopy (CLSM) was used to image *P.putida* in three dimensions while it remained alive and fully hydrated (Schlafer & Meyer, 2017; Stewart et al., 1995). Samples were first dyed by sequentially applying SYTO9 and Concanavalin A (ConA) dyes as described by De León (Rocha Díaz De León, 2021). The selection of fluorescent dyes allowed CLSM imaging to target different aspects of a biofilm, SYTO9 binds to nucleic acids, while ConA is a lectin that targets the EPS by binding to α-mannopyranosyl and α-glucopyranosyl residues (Invitrogen, 2006; Life Technologies, 2014). Samples were stained with each dye in series and, after a mixing period, were rinsed to remove unbound dye and reduce background noise (Artyushkova et al., 2016).

Dyed samples were imaged on a Zeiss LSM 700 confocal microscope, which was equipped with a 63×1.4 NA oil emersion objective. Fluorophores in the SYTO9 and ConA dyes were excited with 2% laser intensity at 488 nm and 366 nm, respectively. The emission wavelengths (498 nm for SYTO9 and 647 nm for ConA) were recorded for each point in a two-dimensional (2D) array (Wilson et al., 2017). By exciting the two wavelengths in series, information from the fluorescent dyes could be recorded on separate channels to minimize crosstalk. For ease of viewing, signal the SYTO9 dye was assigned a green color, and ConA was assigned a red color. CAC particles were visualized using transmitted light. Images were captured in 2048×2048 pixel resolution.

A confocal image stack consists of a series of 2D images collected at different depths by automatically moving the sample stage and, therefore, the focal plane, a set distance between images. Image stacks were acquired using the z-stack function with a step size of 1 μm between each scan plane. The thickness of the in-focus area in each image, as well as the observed fluorescence intensity, are dependent on the microscope's pinhole size. In this research, the

pinhole size was set to 1 Airy unit, which is optimal for fluorescence with the objective used as it provides a balance between depth discrimination and detection efficiency (Carl Zeiss MicroImaging GmbH, 2011; Sekar et al., 2002).

The CLSM gain and digital offset determine the voltage of the photomultiplier and, as a result, the image contrast and brightness (Carl Zeiss MicroImaging GmbH, 2011). The digital offset determines the contrast (blackness) of the background and was set using the "Set Exposure" function for all samples. The "Set Exposure" function also optimized gain for each sample by running an optimization function that balances the number of overexposed and underexposed pixels. For all biofilm-containing samples, "Set Exposure" was used to automatically determine the appropriate imaging parameters.

It was also important to image bacteria-free particulates, as interference can be caused by natural autofluorescence. Autofluorescence introduces uncertainty by producing a detectable signal at the emission wavelength resulting in an indistinct image where the dyed components cannot be decerned from the background (Azeredo et al., 2017). To quantify the degree of autofluorescence from CAC and silica sand, bacteria-free samples were dyed and imaged using the same procedure as bacteria-containing samples. Because the dye procedure requires particles to settle so that excess dye can be rinsed, a saturated solution of calcium chloride ($CaCl_2$, Sigma Aldrich, Darmstadt, Germany) in MilliQ water was added to CAC-containing samples to induce settling, as the CAC particles are too small to settle naturally. When setting imaging parameters for samples without bacteria, the "Set-Exposure" function was run to set the digital offset, but the gain was set to the average values used for biofilm-containing samples. The gain was set manually because, in samples without dyed cells or EPS, the "Set Exposure" function optimized the gain based only on the random noise resulting in inaccurate images.

Image Analysis

Following acquisition, images were processed using the ImageJ software with COMSTAT plugin. First, salt and pepper noise was removed from each image using the inbuilt despeckle filter. The despekle filter is a median filter which replaces each pixel with the mean value of the pixels surrounding it in a 3x3 grid (Ferreira & Rasband, 2012). The Bio-Formats Exporter function was then used to convert the image file to the standardized tagged image file format (TIFF) so that it could be uploaded to the COMSTAT plugin (Linkert et al., 2010).

Within the COMSTAT plugin, thresholding of the image was completed automatically using the Otsu method. Thresholding of an image stack results in a matrix in which pixels with an intensity above the threshold are designated as biomass and given a value of unity and pixels below the threshold are designated as background and given a value of zero (Heydorn et al., 2000). The use of automatic thresholding, such as the Otsu method, is recommended as it reduces error when compared to manual threshold selection (Beyenal et al., 2004; Yang et al., 2001).

For qualitative interpretation, image stacks collected using CLSM were condensed into single images showing the maximum or minimum intensity measured at each pixel throughout the stack. Minimum intensity projections are used for visible light because particulates appear as dark on a light background. Maximum intensity projections were used for the SYTO9 and ConA dye layers because they appeared as light on a dark background.

For quantitative analysis, average biomass thickness (which represents the amount of biofilm present) and roughness coefficient (which indicates the heterogeneity of the biofilm) were calculated using COMSTAT software. Average biofilm thickness was calculated by averaging the thickness of biofilm at each pixel with a signal above the threshold; areas with no fluorescence

were excluded from the calculation. Thickness was calculated at each pixel by subtracting the height of the substratum from the height of the highest slice of the image stack with a detected signal. Voids within the biofilm were ignored and thickness values were averaged across all the pixels in which biofilm was detected. The roughness coefficient is a dimensionless value representing the variability of the thickness of a biofilm. The roughness coefficient was calculated using the following equation 6 where R_a is the roughness coefficient, N is the number of pixels where the thickness was measured, L_{fi} is the individual thickness measured at a given pixel, and $L_{f\,AVE}$ is the average thickness (Heydorn et al., 2000).

$$R_{\mathrm{a}} = \frac{1}{\mathrm{N}} \sum_{\mathrm{i}=1}^{\mathrm{N}} \frac{|\mathrm{L_{fi}} - \mathrm{L_{f\,AVE}}|}{\mathrm{L_{f\,AVE}}} \tag{6}$$

PFAS Analysis

PFOS and PFPeA were analyzed by Liquid Chromatography-Tandem Mass Spectrometry (LC-MS/MS). To prepare samples for analysis, CAC was separated by centrifugating a 13 mL aliquot at 230,000 RCF for one hour, using an Optima XPN series ultracentrifuge (Beckmann Coulter). Centrifuge tubes were rinsed twice with the sample prior to use to minimize loss of PFAS by adsorption to the tube walls (Gilak Hakimabadi et al., 2023).

Following centrifugation, the supernatant was diluted between 5 and 100 times with LCMS grade water and LCMS grade methanol such that the final sample contained 50/50 methanol/water. PFAS analysis was performed using a Shimadzu Tripple Quadrupole Mass Spectrometer operating in negative electrospray with a Thermo Scientific™ Acclaim 120 Å C18, 4.6x 10 mm, 5 µm guard column and an Agilent Infinity Lab Poroshell 120 Å EC-C18, 3.0x5.0 mm, 2.7 µm main column. Two eluents were used, a 5 mM ammonium acetate solution in LCMS grade water and LCMS grade methanol. Further information on the analytical method is described by Gilak Hakimabadi et al. (Gilak Hakimabadi et al., 2023).

Calibration curves were generated for PFOS and PFPeA for a concentration range of 0.05 – 20 and 1 – 20 µg/L, respectively. Based on the slope of the calibration curve, the area ratio of the analyte PFAS and isotopically labelled internal standard PFAS can be converted to the ratio of concentrations. The analyte concentration can then be calculated based on the known concentration of the internal standard. The limit of quantitation for this method was 0.05 µg/L for PFOS and 1 µg/L for PFPeA.

The concentration of sorbed PFAS was then calculated using the equation 6 where C_s is the sorbed concentration in (mg PFAS/g CAC), V is the volume of the reactor (mL), m_A is the mass of CAC (g), $C_{w,o}$ is the initial concentration of PFAS (mg/L), and C_w is the concentration of PFAS measured by LC-MS/MS in the liquid phase after 72 hours of mixing (mg/L) (Worch, 2021).

$$C_s = \frac{V}{m_A}\left(C_{w,0} - C_w\right) \tag{6}$$

3.2.6 Statistical Methods

The difference in sorption between multi-point three-day adsorption experiments was based on the linear adsorption parameter (K_d) using a two tailed t-test at a 95% significance level. Because experiments were performed at different times, there was variation in the concentration of the working stock solution likely due to sorption of PFAS onto the container sides and evaporation of methanol over time. To compare results in cases where the initial concentration varied slightly the K_d was used because it represents the ratio between the sorbed and aqueous phase concentrations. A linear model was selected to facilitate ease of comparison between experiments and may not represent the best fit model in all cases. The K_d values for multi-point experiments were calculated using a regression analysis and the model fit is represented by the R^2 value.

Chapter 4: Results and Discussion

4.1 Characterization of *Pseudomonas Putida*

4.1.1 Growth

The growth of *P.putida* was examined to inform the incubation time required in subsequent experiments. The length of the lag and exponential growth phases of *P.putida* grown in AGW in the absence of CAC was inferred from the OD-time and pH-time profiles for microcosms with a high (80 mg/L) and low (3 mg/L) initial broth concentration. *P.putida* was then incubated in the presence of CAC and the profiles were compared to determine if CAC impacted the growth phase profiles.

In the absence of CAC, the solution OD increased only slightly during the first day, from 0.020 to 0.082 and 0.009 to 0.020 in the experiments with high and low broth concentrations, respectively (Figure 4-1A). The minimal change is suggestive of the lag phase where bacteria adjust to the conditions of the microcosm and prepare for growth. For the high broth microcosms, the solution OD then increased from 0.082 to 0.220 between Day 1 and 3, indicating that *P.putida* entered the exponential growth phase where the bacteria proliferated rapidly. Between Day 3 and 5, a limited change in OD from 0.220 to 0.180 was observed, suggesting that by Day 3 the stationary phase of growth had been reached such that the rate of bacterial growth approximately equaled the rate of death. In the low broth concentration microcosms, the exponential phase of growth appeared to occur over a period of four days, with OD increasing from 0.02 to 0.051 between Day 1 and 3, and from 0.051 to 0.069 between Day 3 and 4. Between Day 4 and 8, the OD in the low broth microcosms only increased slightly from 0.069 to 0.099, suggesting that the growth of *P.putida* had reached the stationary phase.

The more rapid growth and greater OD in the high broth concentration microcosms can be attributed to the nutrients available in the media and the concentration of cells in the inoculum. Broth is a complex media that is recommended for the growth of *P.putida* and, as such, provides the carbon and salts needed in an easy-to-utilize form to allow the bacteria to grow rapidly. On the other hand, AGW is a defined media that contains the carbon and salts required for bacterial growth in lower concentrations and harder-to-utilize form. When the concentration of broth in the microcosm was increased from 3 mg/L to 80 mg/L, the rate of *P. putida* growth increased as shown by the shortened exponential growth phase. The increased growth rate of the bacteria in broth may have also allowed more cells introduced in the inoculum of the high broth concentration microcosm (8 g/L broth) than in the low broth concentration inoculum (48 mg/L broth) despite different inoculum volumes being used. The differences in initial cell concentrations and growth rates resulted in more bacteria being produced and thus a higher final OD in the high broth concentration microcosms.

The change in the solution pH (Figure 4-1B) mirrored the OD change. A slight increase in pH, from 7.0 to 7.3 for high broth and from 7.0 to 7.4 for low broth concentration, was observed during the first day of the experiment. Between Day 1 and 3, the solution pH increased more substantially, from 7.3 to 8.2 and 7.4 to 8.0 in the high and low broth concentration experiments, respectively. In the low broth concentration microcosms, the solution pH increased to 8.2 after Day 4 while the pH of the high broth concentration microcosm remained constant.

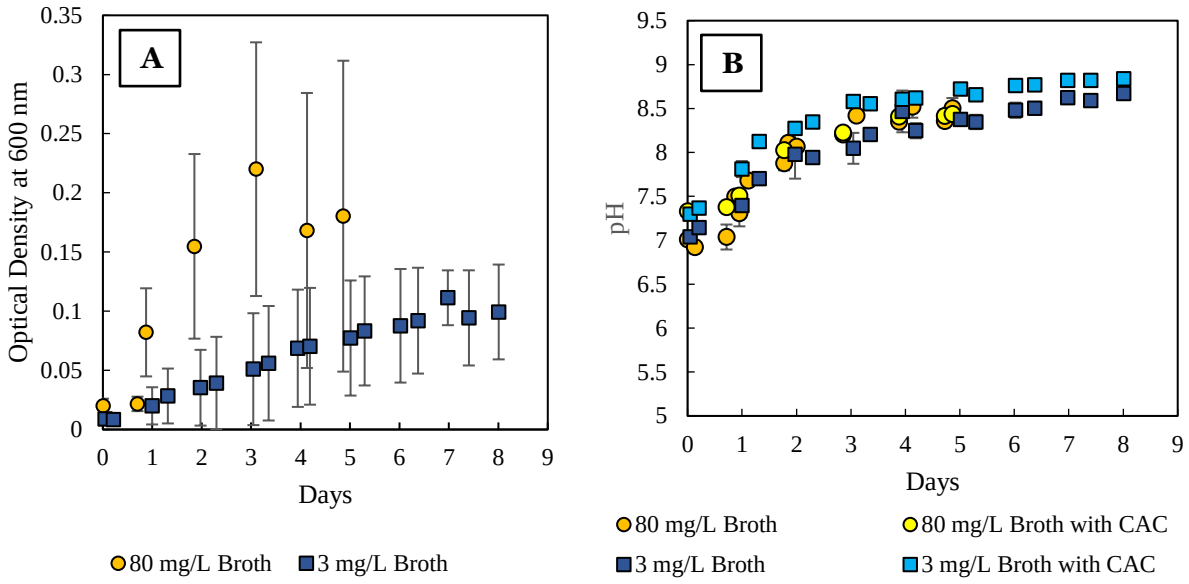


Figure 4-1: Growth of P.putida in 50 mL AGW containing 3 mg/L or 80 mg/L beef broth as indicated by A) Optical Density and B) pH. Vertical error bars represent one standard deviation of three replicate measurements.

Because the solution OD could not be measured when CAC was present, the growth of *P.putida* was deduced from the solution pH (Figure 4-1B). As in the CAC-free system, the solution pH in the CAC-containing microcosms slightly increased during the first day, from 7.3 to 7.5, and from 7.3 to 7.8 in the high and low broth concentration experiments, respectively. Between Day 1 and 3, the solution pH in the high broth concentration microcosms increased from 7.5 to 8.2, while in the low broth concentration microcosms, the solution pH increased from 7.8 to 8.6. The trend of increasing pH was consistent between microcosms with and without CAC, indicating that the presence of CAC did not appear to affect the timing of *P.putida's* growth phases.

The trend of increasing solution pH during the growth of *P.putida* (both in the absence and presence of CAC) is similar to the results obtained by Sánchez-Clemente et al., who observed a decrease in the solution pH during the growth of *P.putida* in the presence of a reduced carbon source (e.g., glucose or glycerol) but a pH increase in the presence of an oxidized carbon source (e.g., citrate and fumarate) (Sánchez-Clemente et al., 2020). In the current study, AGW contained

acetate, which is an oxidized carbon source. The acetate utilization by *P.putida* likely resulted in increased extracellular pH.

4.1.2 Attachment of Biofilm to Colloidal Particles

Five sets of microcosms were used to evaluate the ability of *P.putida* to form biofilm on CAC. Microcosms Sets 1 and 2, which contained dyed CAC and sand, respectively, were used to evaluate the particulate autofluorescence. Microcosm Set 3 contained *P.putida* grown in the absence of particulates and was used as a reference for planktonic bacterial growth. Microcosm Set 4 and Set 5 contained *P.putida* grown in the presence of CAC and sand, respectively.

In microcosms Sets 1 and 2, when *P.putida* was absent, Con A dye (red) fluoresced when associated with CAC (Figure 4-2A), while both Con A dye (red) and SYTO9 (green) fluoresced when associated with sand (Figure 4-2B). The red and green areas on the CLSM images appeared randomly distributed and with no identifiable shape. In contrast, when bacteria was present in Sets 3, 4, and 5, the green areas on the CLSM images were identifiable 1-5 μm rods, corresponding to the shape of a *P.putida* cell (Figure 4-3 and Figure 4-4). The clumping of particles observed in these images is an artifact of the dye process and not representative of the distribution of particulate before dying.

Without any particulate, images of *P. putida* in Set 3 showed little aggregation of cells and EPS dispersed throughout the sample image (Figure 4-3). This suggests that *P.putida* remained in the planktonic state. With the addition of CAC in Set 4, sample image shows an aggregate of bacterial cells, some of which were encapsulated within a red-color layer (Figure 4-4A and C). The presence of the red color areas, which is unlikely the result of CAC autofluorescence, suggests that the bacterial cells were interconnected with EPS. When sand used as the particulate in Set 5 (Figure

4-4B and D), the sample images showed some areas of intense bright green and red similar to the autofluorescence observed in Set 2 (Figure 4-2B). Therefore, much of the fluorescence was attributed to the autofluorescence of the sand particle and no numerical comparison could be made to the biofilm grown on CAC. However, rod shaped bacteria are still visible in some areas of Figure 4-4D in close proximity to the sand particles, indicating that, despite difficulties in imaging, a biofilm does appear to have formed on the fine sand.

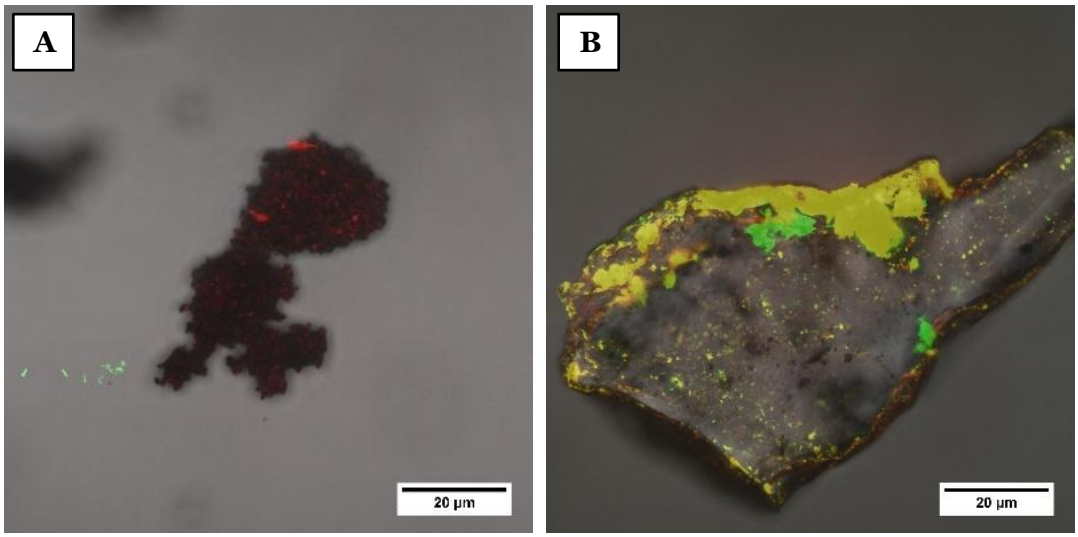


Figure 4-2: CLSM maximum intensity projections of samples from microcosms incubated in the absence of bacteria. (A) Set 1 contained CAC and (B) Set 2 contained fine silica sand. The clumping of particles visibe in these images is an artifact of the dye process and therefore not representative of the bacteria-free particle distribution before dying.

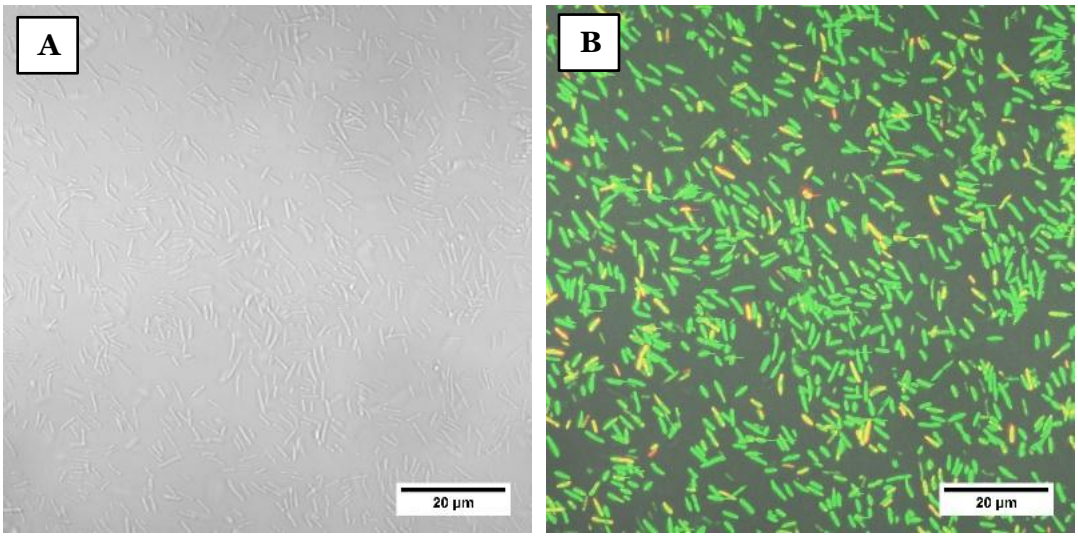


Figure 4-3: Microcosm Set 3: P.Putida incubated in AGW with 80 mg/L broth in the absence of particulate. (A) Images observed under CLSM using only visible light and (B) Overlaying the visible light with a maximum intensity of the fluorescent dyes.

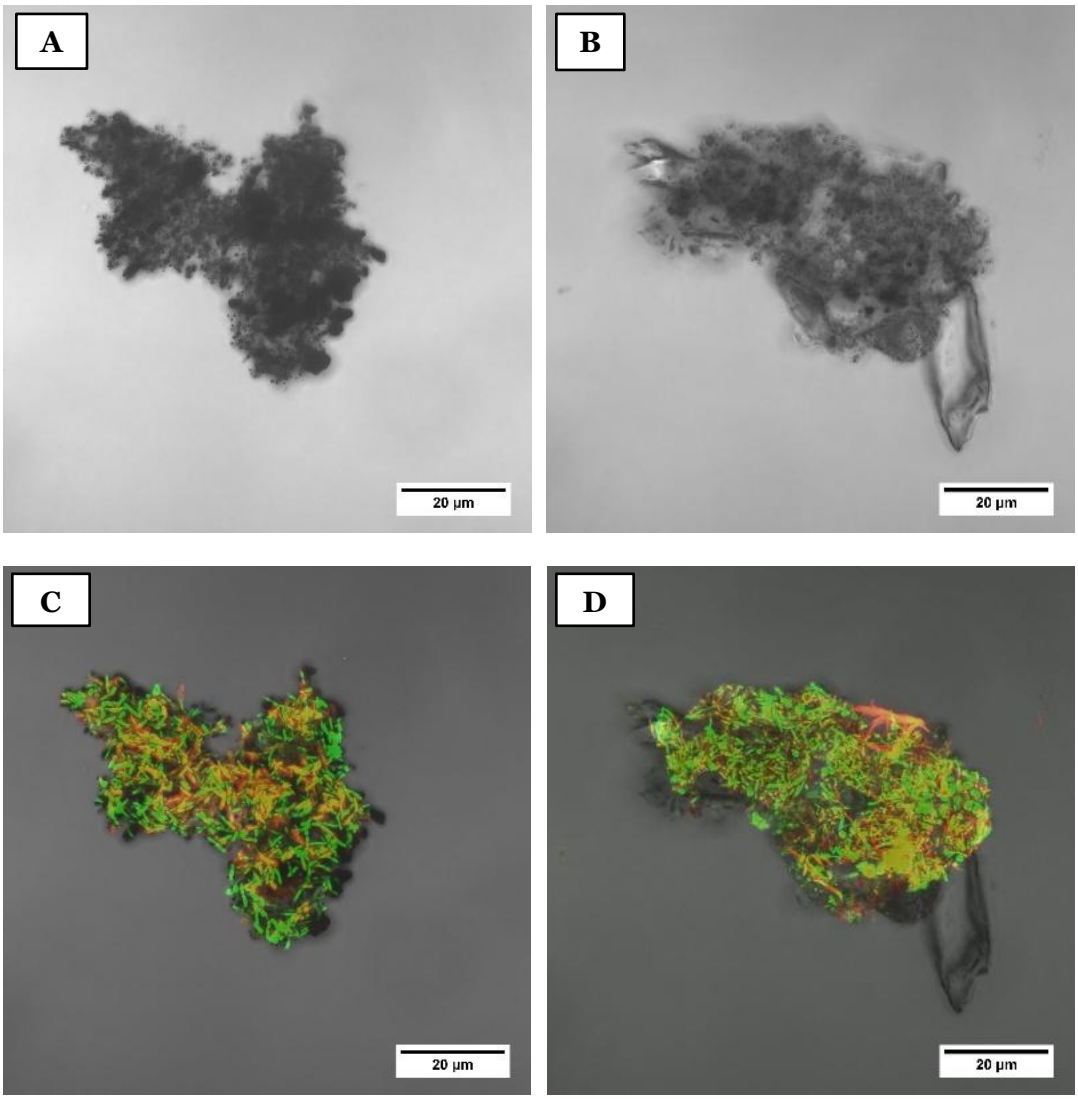


Figure 4-4: Images (A) and (B) show visible light projections of CLSM images of Set 4, bacteria-coated CAC (A) and Set 5, bacteria coated sand (B) incubated in the presence of P.putida and 80 mg/L broth in AGW. The particulate appears as dark grey or black. Images (C) and (D) show visible light projections overlayed with the maximum intensity of the fluorescent dyes for P.Putida-coated CAC (C) and Sand (D). Cells are coloured green and EPS is coloured red.

The CLSM images and the corresponding visible light projections (Fig. 4-4) suggest that the bacterial cells encapsulated an aggregate of CAC or sand particles. Therefore, it is concluded that *P.putida* was able to form a biofilm by incorporating particles (including CAC particles that were

<5 μm) to form a larger agglomerate held together by EPS. Additional images of biofilm formation on sand are presented in Appendix B.

The aggregation of CAC particles was also clearly visible during the incubation period. Figure 4-5A and 4-5B present images of samples collected from the microcosms Set 1 (bacteria free CAC) and Set 4 (*P.putida* containing CAC), respectively. In the absence of *P.putida*, CAC particles remained suspended in solution, whereas the CAC particles incubated with *P.putida* aggregated and settled out of solution in less than 10 min. The rapid settling of CAC incubated with *P. putida* further indicates the ability of the biofilm to aggregate particulate.

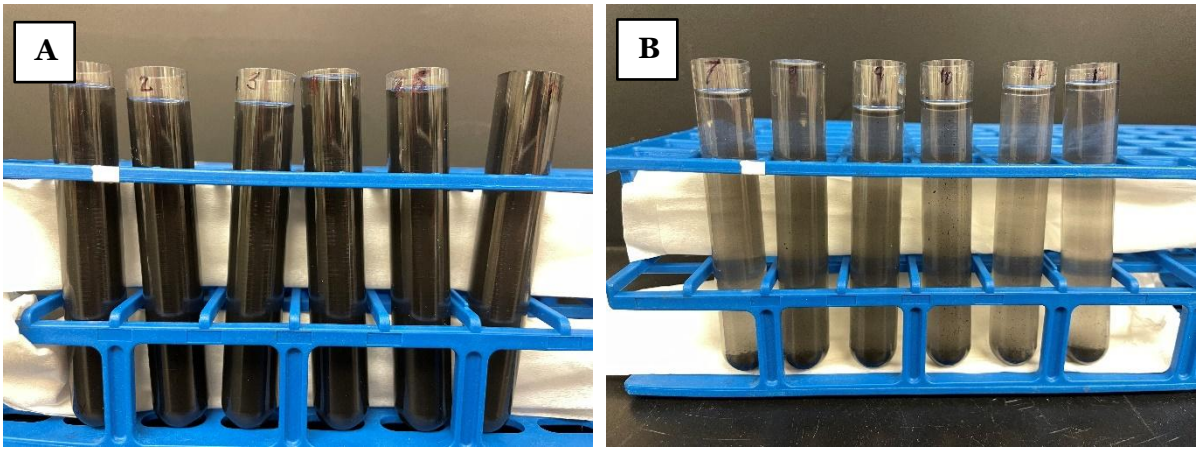


Figure 4-5: Samples from microcosm (A) Set 1, CAC in the absence of bacteria and (B) Set 4, CAC with P.putida collected after the incubation period in AGW with 80 mg/L broth. Samples were allowed to settle for 10 minutes before being photographed.

To further quantify the formation of biofilm in the CAC-containing microcosms, growth was monitored by calculating the biofilm thickness and roughness from CLSM images collected over seven days of growth (Figure 4-6). During the first four days, the biofilm grew quickly to a thickness of 11.0 μm for bacterial cells and 9.0 μm for EPS. The change in biofilm thickness between Day 4 and 7 was minimal, with the thickness of cells decreasing from 11.0 μm to 10.8 μm

and EPS thickness decreasing from 9.0 μm to 8.1 μm. These changes suggest that the exponential phase of growth occurred over the first four days and was followed by the stationary phase, in agreement with the conclusion made based on the solution OD trends (Figure 4-1).

The dimensionless roughness coefficient, which is an indication of biofilm heterogeneity, decreased rapidly between Day 2 to Day 4 (Figure 4-6B), with the roughness of the bacterial cells decreasing from 1.61 at 0.87 and the EPS roughness decreasing from 1.59 to 0.67. During the stationary phase (Day 4 to 7), the change in roughness was less appreciable (from 0.87 to 0.80 for cells and 0.67 to 0.74 for EPS).

The decrease in roughness over time is consistent with the description of *P.putida* biofilm development presented by Tolker-Nielsen et al. (2000). The *P.putida* biofilm is described as first forming independent microcolonies where the cells were present in uneven clumps, resulting in a greater variability in height and, as a result, likely larger roughness coefficient (Tolker-Nielsen et al., 2000). Following the initial microcolony formation, the flagella on the *P.putida* allow the bacteria to rearrange into larger structures that would lead to a decrease in the roughness coefficient as the cells become more interconnected(Tolker-Nielsen et al., 2000). Therefore, the observed decrease in the roughness coefficient over time likely represents the maturation of the *P.putida* biofilm (Stoodley et al., 2002). The rapid initial decrease over four days, followed by a plateau is consistent with a biofilm growing and maturing quickly during the exponential phase, then maintaining its structure during the stationary phase.

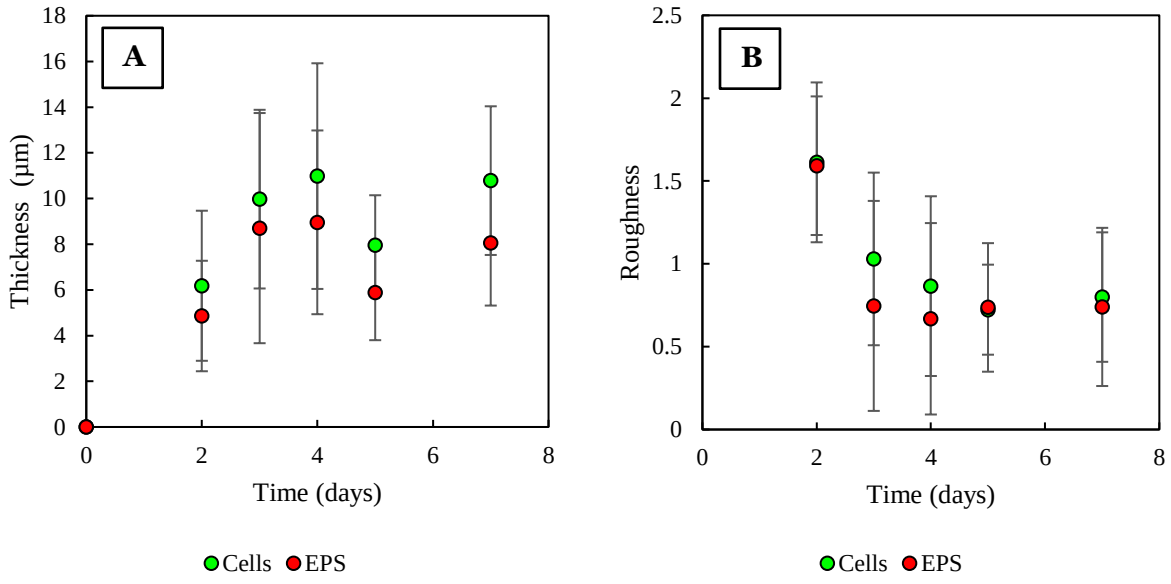


Figure 4-6: Thickness and roughness of biofilm on CAC during growth in a microcosm with 3 mg/L Broth as measured using CLSM. Vertical error bars represent one standard deviation.

In summary, the evidence suggests that *P.putida* is capable of forming a biofilm on CAC particles. Rather than the classical depiction of a biofilm adhered to a single surface, the *P.putida* biofilm formed an aggregate of CAC particles, which were held together by EPS. As the biofilm developed on CAC, it appeared to increase in thickness and decrease in roughness, likely due to the formation of more cohesive structures.

4.2 Impact of Biofilms on PFAS Adsorption

4.2.1 Effect of the concentration of broth on PFOS adsorption and biofilm formation

Previous studies have shown that DOC can diminish PFAS sorption on CAC due to competition for available sorption sites (Gilak Hakimabadi et al., 2023; Molé et al., 2024). As such, prior to investigating the effect of the biofilm formed by *P.putida* on the adsorption of PFAS on CAC, experiments were conducted to assess the adsorption of PFOS on CAC in the absence of *P.putida*.

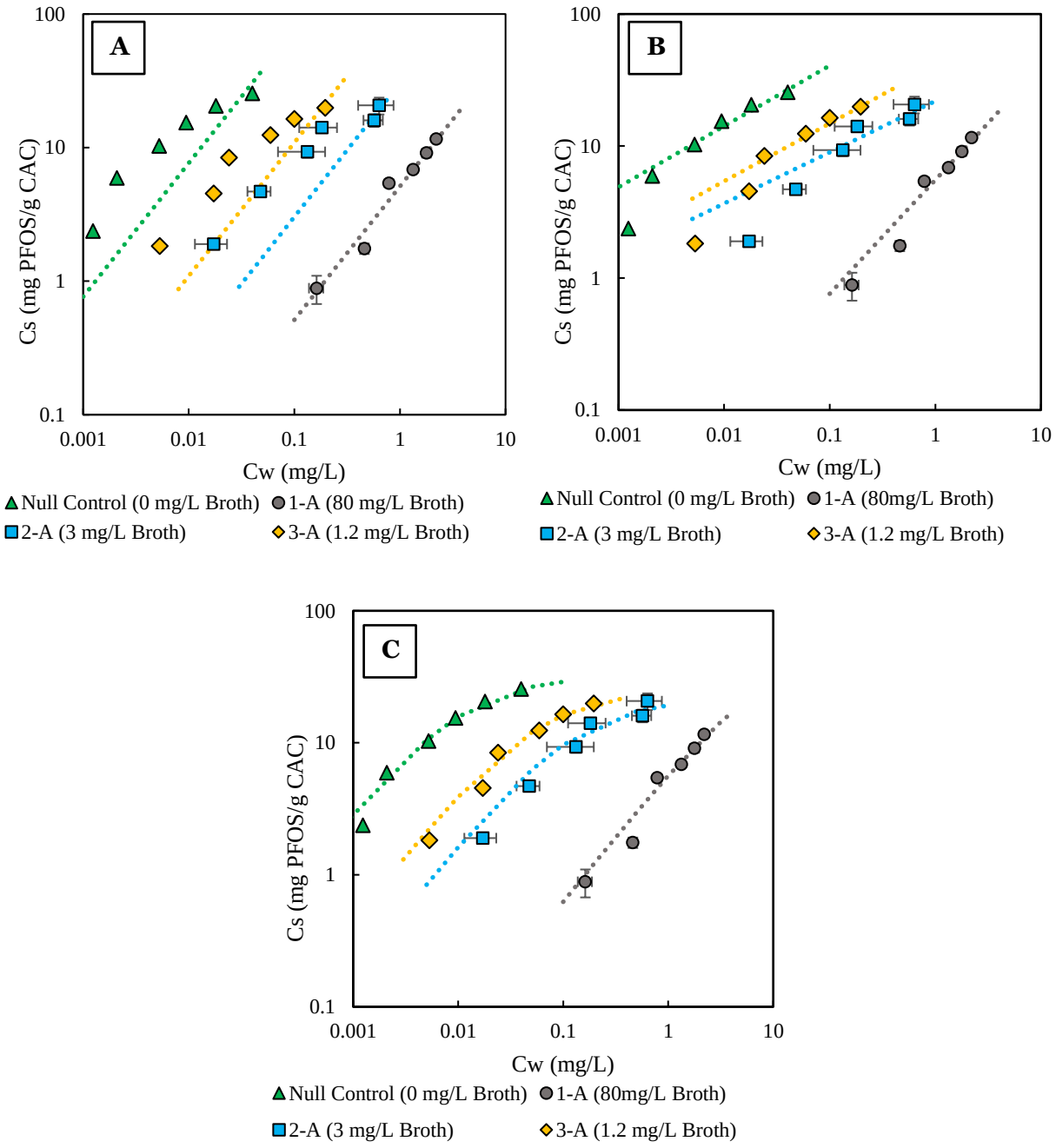


Figure 4-7: The effect of added broth on the adsorption of PFOS to CAC. Reaction solutions contained 0.12 g/L CAC and a starting concentration of 0.26–2.5 mg/L of PFOS. Fitting lines represent (A) a linear model (B) a Freundlich model and (C) a Langmuir model of the data. Fitting parameters are listed Table 4-1. Error bars represent one standard deviation of replicate measurements.

Table 4-1: Parameters for a linear, Freundlich, and Langmuir model fit to the adsorption of PFOS on abiotic CAC in the presence of nutrient broth (Figure 4-7). Error presented is equal to the standard error of the value.

	Linear		**Freundlich**			**Langmuir**		
	K_d (L/g)	**R^2**	**K_f (mg/g)(mg/L)$^{-n}$**	**n**	**R^2**	**K_l (L/mg)**	**C_{smax} (mg/g)**	**R^2**
Null Control	764±105	0.841	118±23	0.46±0.05	0.932	97.9±15.9	31.9±2.0	0.972
3-A (1.2 mg/L)	109±18	0.776	40.7±7.0	0.44±0.07	0.859	18.3±4.4	25.2±2.5	0.940
2-A (3 mg/L)	30.3±3.1	0.769	21.9±1.7	0.39±0.06	0.733	8.11±2.3	21.6±1.9	0.797
1-A (80 g/L)	5.13±0.25	0.951	5.55±0.43	0.86±0.11	0.847	0.13±0.12	50.5±41.3	0.847

Previous studies have suggested that the Freundlich isotherm model represented the adsorption of PFAS on AC. In the current study, the trend between C_s and C_w was better represented by the Langmuir model as shown by R^2 values of 0.972, 0.940, 0.797, and 0.847 for the null control, 3-A, 2-A, and 1-A respectively. (dashed line in Figure 4-7C). Because DOC is able to occupy a fraction of the available sorption sites, the Langmuir model may be able to better represent the data as it assumes a finite number of available sorption sites.

In conjunction with the abiotic experiments, experiments containing *P.putida* were conducted to assess the effect of the broth concentration on the development of biofilm on CAC. The CAC aggregates formed in the microcosm containing the lowest broth concentration (1.2 mg/L) were the smallest, while the aggregates formed in the microcosms containing a broth concentration of 3 and 80 mg/L were similar in size, with the biofilm layer formed in the 80 mg/L broth microcosm appearing to be denser (Figure 4-8). In the experiment containing 80 mg/L of broth, the biofilm thickness ranged between 3.00 and 23.42 μm for bacterial cells, and between 1.94 and 19.89 μm for EPS, while the roughness coefficient ranged between 1.95 and 2.00. As the initial concentration of broth was decreased to 3 and 1.2 mg/L, the thickness of the bacterial cells and EPS, as well as the roughness coefficient, also decreased (Table 4-2, Figure 4-9). This result

indicates that in the presence of higher broth concentrations, *P.putida* produced a thicker biofilm layer that matured into a smoother structure.

Table 4-2: Thickness and roughness of P.putida biofilm grown on CAC particles. Error represents the standard deviation of the values

	Cells		**EPS**	
	Thickness **(µm)**	**Roughness**	***Thickness*** **(µm)**	**Roughness**
3-P (1.2 mg/L)	4.7±2.5	1.96±0.05	3.6±1.7	2.00±0.01
2-P (3 mg/L)	5.3±2.2	1.79±0.21	4.6±2.0	1.81±0.21
1-P (80 g/L)	9.9±5.9	1.35±0.46	7.1±4.3	1.31±0.49

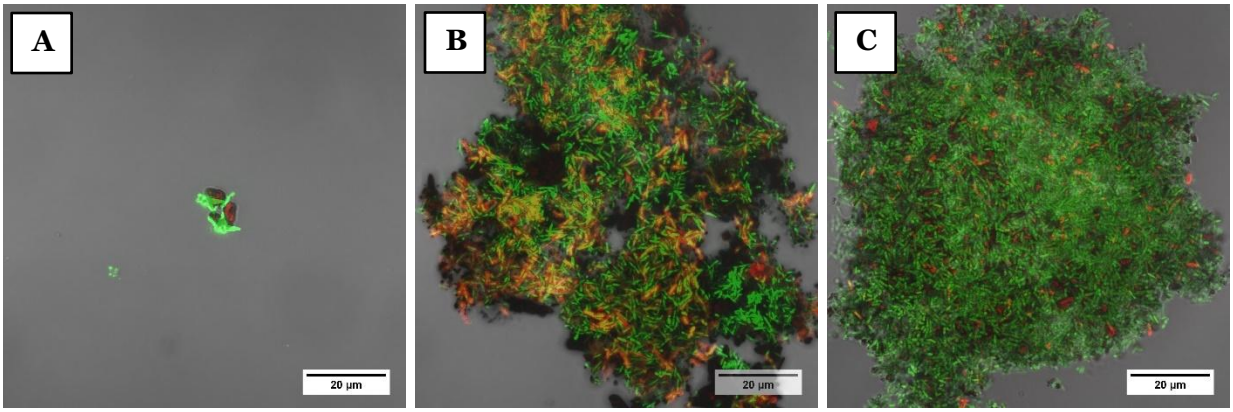


Figure 4-8: Biofilm formation on CAC after seven days of incubation in AGW for experiments A) 3-P (1.2 mg/L broth) B) 2-P (3 mg/L) broth and C) 1-P (80 mg/L broth)

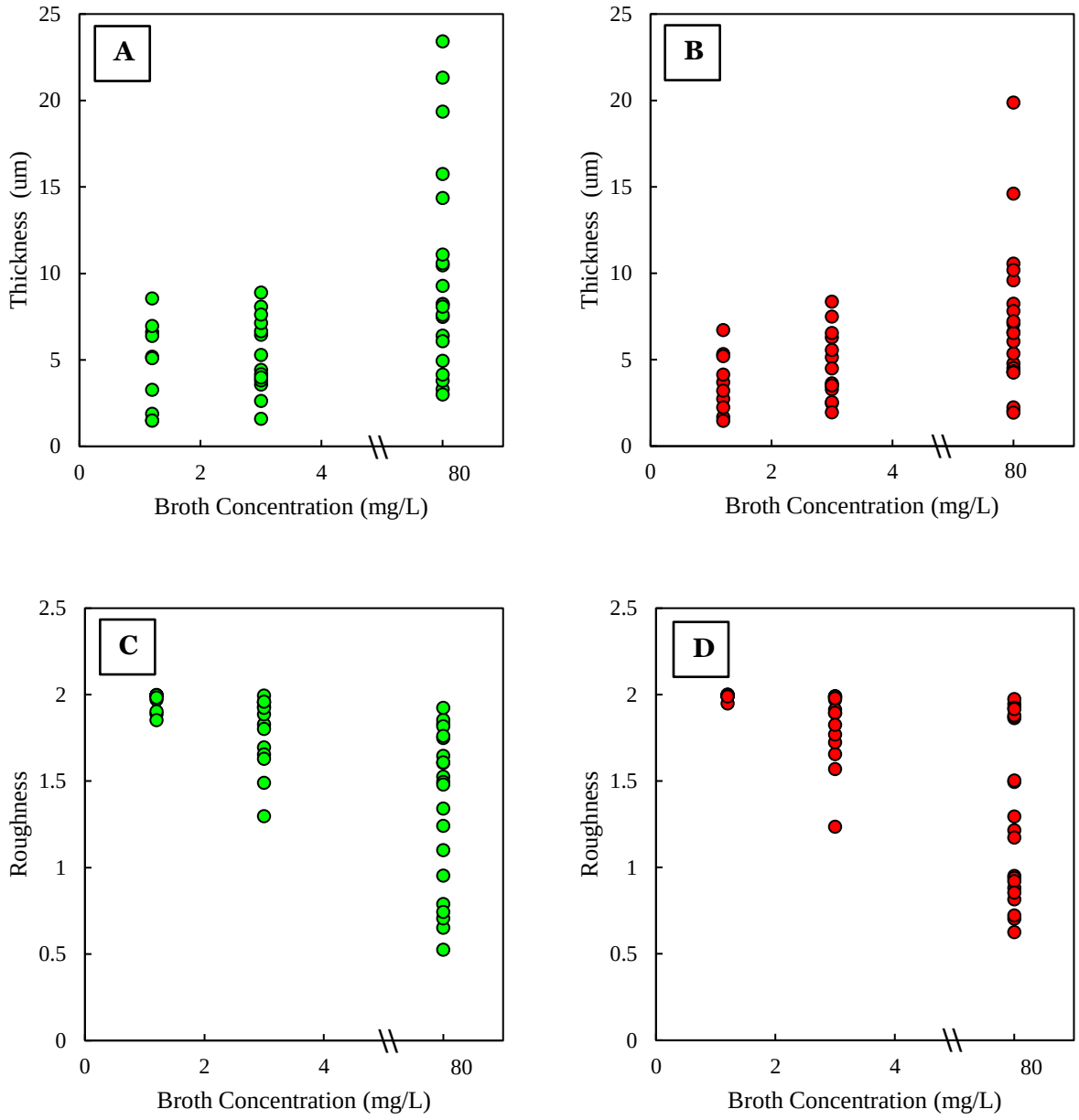


Figure 4-9: Variation in biomass thickness, and roughness of P.Putida biofilm grown in experiments 1-P, 2-P, and 3-P, after seven days. Each point represents the value of an individual image. Values for cells are shown in green, values for EPS are shown in Red.

In summary, it was observed that a high initial broth concentration (i.e., 80 mg/L) significantly suppressed the adsorption of PFOS on CAC. Because this effect of broth may mask the effect of biofilm on PFOS adsorption, experiments investigating the effect of biofilm should employ a low

broth concentration but sufficient to support *P.putida* growth and biofilm formation. When the initial concentration of broth was 1.2 mg/L, the biofilm formed after four days did not appear to be fully developed (Figure 4-8 and Figure 4-9). Based on these considerations, subsequent sorption experiments investigating the adsorption of PFOS and PFPeA on CAC in the presence of *P.putida* were performed with an initial broth concentration of 3 mg/L (low) and 80 mg/L (high).

4.2.2 Adsorption Kinetics

In experiments investigating the adsorption of PFOS and PFPeA on CAC in the absence or presence of *P.putida*, the aqueous phase concentration (C_w) of these compounds were monitored over five (PFOS) and eight days (PFPeA) to determine the time to adsorption equilibrium (Figure 4-10).

With PFOS, a significant decrease in C_w occurred over the first three days, from 0.65 to 0.063 mg/L and 0.65 to 0.153 mg/L in the bacteria-free and bacteria-containing systems, respectively. Between Day 3 and Day 5, the adsorption of PFOS appeared to slow, with the average C_w decreasing only slightly from 0.063 to 0.050 mg/L in the bacteria-free microcosm and varying in the *P.putida* containing microcosm from 0.153 mg/L on Day 3 to 0.115 mg/L on day 4, and back to 0.153 mg/L on day 5. Bacteria-free and *P.putida* containing microcosms appeared to reach sorption equilibrium by day 3 resulting in an initial sorption rate of 0.010 mg/day for the biofilm-free system and 0.008 mg/day in the *P.putida* containing system. At equilibrium, 92% of the PFOS mass added to the bacteria-free system was removed from the solution, while 76% was removed in the *P.putida*-containing system.

The difference in PFOS removal between the two systems was determined to be statistically significant at the 95% confidence level. The decrease in adsorption in the presence of *P.putida* is

presumed to be due to biofilm blocking sorptive sites. For a PFOS molecule to adsorb to CAC, the PFOS molecule must first diffuse through a layer of water surrounding the particle (external diffusion), then through the pore spaces to an available sorption site (internal diffusion) (Worch, 2021). When a biofilm is present, it would be expected that the external diffusion of the PFOS molecule would slow as the PFOS diffuses through the biofilm structure. In contrast, internal diffusion may occur at the same rate with and without a biofilm as the bacteria (approximately 1 μm in size) do not fit within the pores of a CAC particle (<0.05 μm). The results show that the majority of PFOS sorption occurred within the first three days, regardless of whether a biofilm was present or not (Figure 4-10). The slight difference in initial adsorption rate (0.010 mg/day for bacteria-free and 0.008 mg/day for *P.putida* containing) suggests that the decrease in PFOS adsorption rate was only influenced to a small extent by a slower rate of external diffusion when biofilm was present. Instead, the decreased sorption may be influenced to a greater extent by competitive sorption between PFOS and extracellular molecules (e.g., proteins excreted by the bacteria).

Compared to PFOS, PFPeA was not removed appreciably. In the bacteria-free microcosms, C_w decreased from 0.398 to 0.364 mg/L over the first three days and remained essentially unchanged by Day 5. In the bacteria-containing microcosms, C_w decreased from 0.398 to 0.367 mg/L within the first three days, increased slightly to 0.385 mg/L by Day 5, and remained steady on Day 8. Overall, only 15% and 11% of the added PFPeA mass was removed from the solution in the bacteria-free and bacteria-containing systems, respectively. The differences in PFPeA mass removal between the two systems were not statistically significant at a 95% confidence level; therefore, the results were not fit to a kinetic model. The observed limited sorption of PFPeA is consistent with the finding that compounds with shorter fluorinated chain lengths have lower

affinity to AC (Gilak Hakimabadi et al., 2023; G. Kim et al., 2024; Mccleaf et al., 2017; Molé et al., 2024).

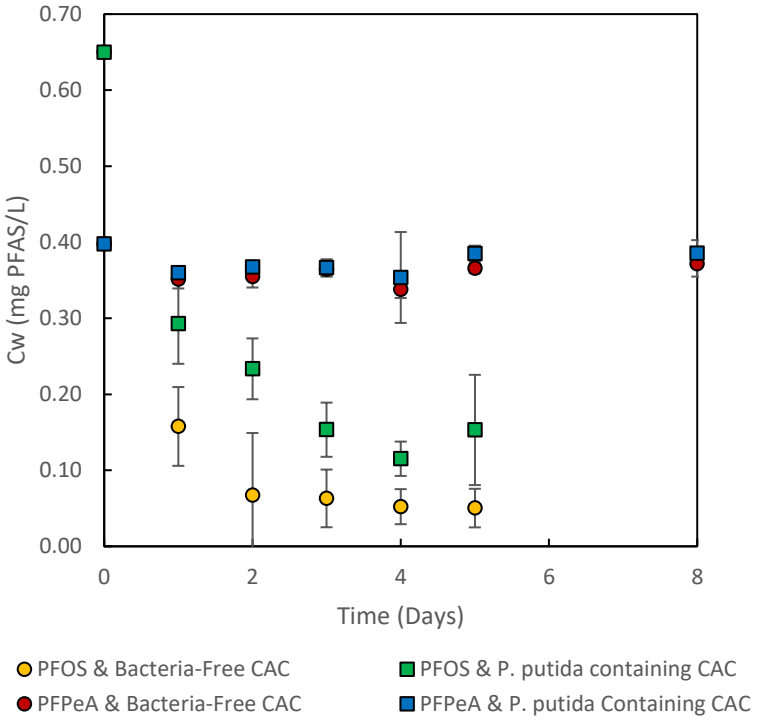


Figure 4-10: *PFAS adsorption on biofilm-free and biofilm-coated CAC over 5 to 8 days. Reaction solutions contained 0.12 g/L CAC, 3 mg/L broth, and 0.65 mg/L PFOS or 0.398 PFPeA. Error bars represent one standard deviation of replicate measurements.*

The adsorption of PFOS to bacteria-free and *P.putida* containing CAC was represented using first order and pseudo-second order kinetic equations (Figure 4-11 and Table 4-3). The first order kinetic coefficient was equal to 0.072 h^{-1} and 0.049 h^{-1} for bacteria-free and bacteria containing CAC respectively. The pseudo-second order coefficient was equal to 0.056 $g \cdot mg^{-1} \cdot h^{-1}$ for bacteria-free CAC and 0.038 $g \cdot mg^{-1} \cdot h^{-1}$ for *P.putida* containing CAC. In both approaches, the addition of bacteria resulted in a 70% decrease in the kinetic coefficient, indicating that the presence of bacteria decreases the rate at which PFOS is able to sorb. A comparison of R^2 values indicates that the results were best represented with first order kinetics; however, previous studies have

found that pseudo-second order kinetics are more representative of PFOS sorption to activated carbon (Chen et al., 2017; Grieco et al., 2021; G. Kim et al., 2024). This difference in kinetics is likely due to limited early time data in the kinetic experiments conducted. As a result, data is not available for the time that the sorbed concentration is changing most rapidly resulting in the the application of first and second order kinetic to deviate from the results obtained in previous experiments.

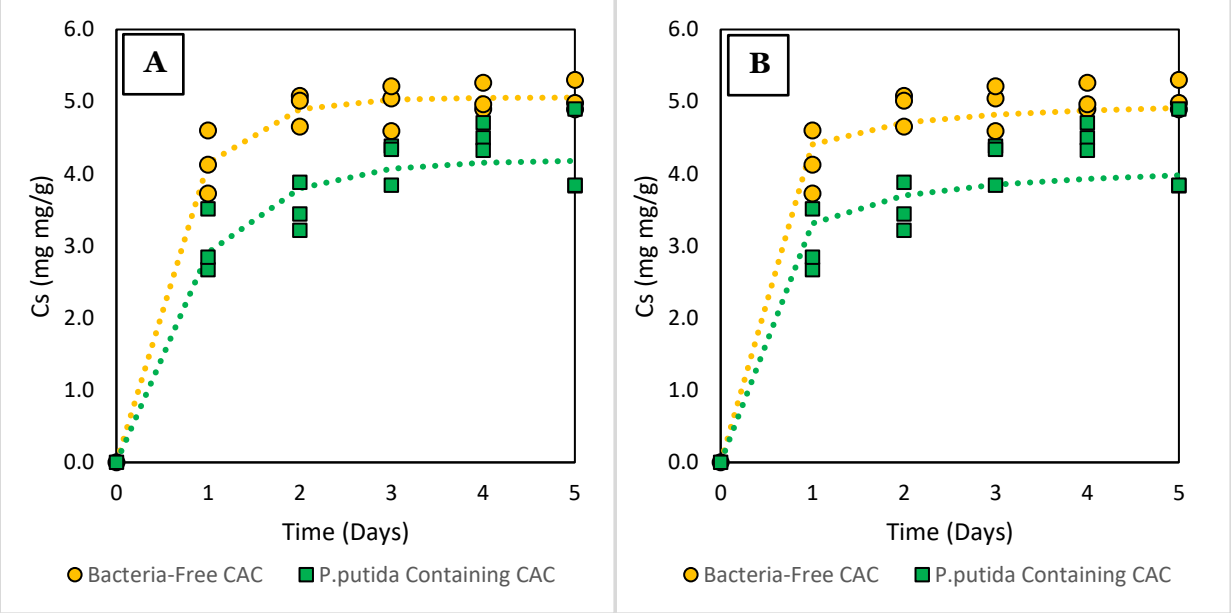


Figure 4-11: Adsorption kinetics of PFOS sorption to bacteria-free and P.putida containing CAC wit with (A) a first order kinetic model and (B) a pseudo-second order kinetic model. Fit parameters are listed in Table 4-3.

Table 4-3: Kinetic coefficients for the adsorption of PFOS to bacteria-free and P.putida containing CAC (Figure 4-11)

	First Order Kinetics		Pseudo-Second Order Kinetics	
	k_1 (h^{-1})	R^2	k_2 ($g \cdot mg^{-1} \cdot h^{-1}$)	R^2
Bacteria free CAC	0.072	0.96	0.056	0.94
P.putida containing CAC	0.049	0.86	0.038	0.76

In the kinetic experiment, after PFOS or PFPeA was added, the change in the biofilm thickness and roughness were monitored daily (Figure 4-12 and 4-12). Limited variation in the thickness of

the biofilm was observed, with the average thickness of cells ranging from 6.6 to 10.4 μm and the average EPS thickness ranging from 6.6 to 10.8 μm. Similarly, both cell and EPS roughness coefficients remained relatively constant, ranging from 1.43 to 1.73 (cell roughness) and 1.45 to 1.76 (EPS roughness). The constant thickness and roughness of the biofilm over the course of the experiment indicates that the biofilm remained in the stationary phase of growth where cells within the biofilm are being produced at approximately the same rate as they are dying and being removed. Because the characteristics of the biofilm remained constant, it appears that the presence of PFOS did not influence the biofilm structure. As a result, changes to the biofilm layer are not expected to significantly affect the adsorption of PFOS or PFPeA to CAC under the conditions employed.

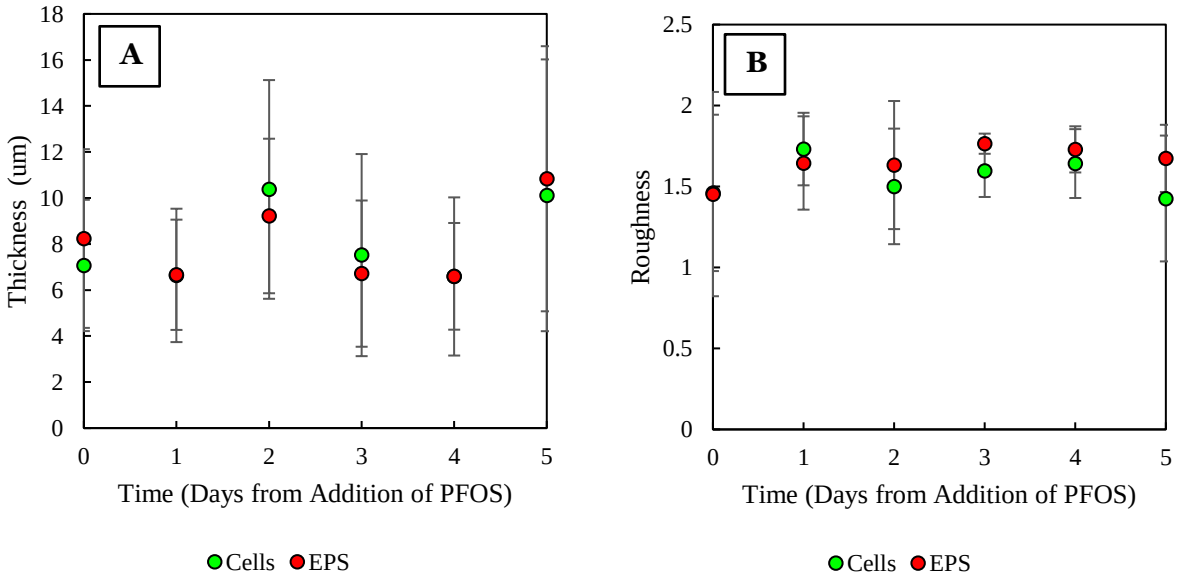


Figure 4-12: Average thickness and roughness of cells and EPS measured during 5-day kinetic PFOS adsorption experiment. Reaction solutions contained 0.12 g/L CAC, 3 mg/L broth, and 0.65 mg/L PFOS in AGW with 3 mg/L broth. Vertical error bars represent one standard deviation.

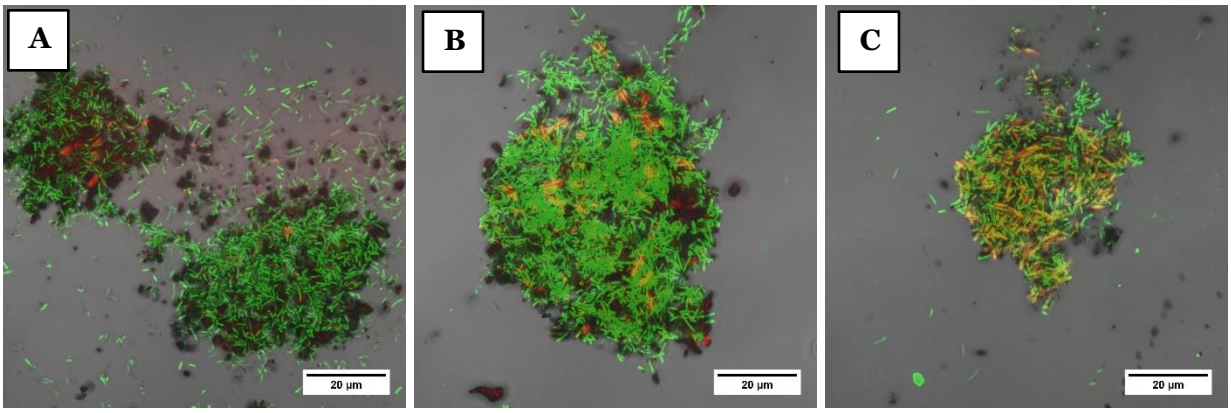


Figure 4-13: Biofilm formation on CAC particles after (A) 1 day, (B), 3 days, and (C) 5 days in contact with PFOS during the kinetic experiment. Reaction solutions contained 0.12 g/L CAC, 3 mg/L broth, and 0.65 mg/L PFOS in AGW with 3 mg/L broth. Additional images of the biofilm during the kinetic experiment are presented in Appendix B.

4.2.3 Effect of biofilm on the adsorption of PFOS and PFPeA at different aqueous phase concentrations

The effect of biofilm on the adsorption of PFOS and PFPeA by CAC was further evaluated at different initial C_w. For this purpose, following the period of *P.putida* incubation with CAC (four days), different amounts of PFOS or PFPeA were added to the reaction solution to obtain an initial concentration ranging from 0.5 to 5 µM (i.e. 0.26–2.5 mg/L for PFOS or 0.14 –1.4 mg/L for PFPeA). Subsequently, the microcosms were incubated for another three days and subsampled for PFAS analysis. Based on the results of the kinetic experiment described in the previous section, the adsorption of PFOS and PFPeA was assumed to attain equilibrium after three days.

Data from the bacterial control experiment (i.e., *P.putida* grown in the absence of CAC) suggests that PFOS did not adsorb appreciably to the bacterial cells, with the partition coefficient K_d ranging between 0.19 and 0.73 L/g (Figure 4-14 and Table 4-2). The calculated K_d values for PFOS sorption were are an order of magnitude higher than those obtained of obtained by Butzen et al. (0.019 L/g) for sorption to *P.putida* but similar in magnitude to those obtained by Dai et. al.

(0.253 L/g) for sorption to a similar, gram-negative bacteria, *Pseudomonas aeruginosa* (Butzen et al., 2020; Dai et al., 2023). Despite variation in reported and measured K_d values, the sorption of PFOS to bacteria is notably less than to CAC in the absence of *P.putida* under the same conditions (5.13 L/g) and is therefore unlikely to appreciably effect the extent of sorption measured in *P.putida* containing microcosms.

In the presence of CAC but the absence of *P.putida*, K_d ranged from 4.33 to 7.69 L/g and 29.5 to 122.1 L/g for microcosms containing an initial broth concentration of 80 mg/L and 3 mg/L respectively. As mentioned previously, components in the broth compete with PFOS for adsorptive sites on CAC, and the higher concentration of broth resulted in a decrease in PFOS adsorption. The difference in the adsorption of PFOS between bacteria-free and *P.putida* containing CAC was statistically significant at a 95% confidence level. When both *P.putida* and CAC were present, the amount of PFOS removed from the solution decreased compared to the bacteria-free CAC system, with K_d ranging between 0.18 and 2.28 L/g (80 mg/L broth microcosms), and between 9.96 and 38.13 L/g (3 mg/L broth microcosms). The decreased sorption of PFOS by CAC in the presence of *P.putida* can be attributable to the effect of biofilm, as discussed previously. Because kinetic experiments were conducted in 3 mg/L broth microcosms, it is unknown if the 80 mg/L broth microcosm has reached adsorption equilibrium. If this is the case, a smaller difference in PFOS sorption between bacteria-free and *P.putida* containing CAC may be observed The decreased sorption may also be due in part to the solution pH in the *P.putida*/CAC system being slightly lower. In particular, the solution pH was approximately 7 in the microcosms containing CAC but no *P.putida*, whereas the pH in the *P.putida*/CAC system was 7 at the beginning of the experiment and increased to 8.5 by the end of the experiment. A trend of decreasing PFOS sorption to activated carbon with increasing pH has been well documented, although the influence of pH on PFOS adsorption is less pronounced in

higher ionic strength solutions, such as the AGW (ionic strength of 5.57 mM) used (Du et al., 2014).

Table 4-4: K_d values for bacteria free CAC, P.putida containing CAC, and P.putida in the absence of CAC as shown by linear data fit on Figure 4-14 and Figure 4-15

	Conditions	**K_d** L/g
Bacterial Control	PFOS, no bacteria, no CAC, 80 mg/L broth	0.19-0.73
1-A	PFOS, no bacteria, 80 mg/L Broth	4.33-7.69
1-P	PFOS, *P.putida*, 80 mg/L Broth	0.18-2.28
2-A	PFOS, no bacteria, 3 mg/L Broth	29.5-122.1
2-P	PFOS, *P.putida*, 3 mg/L Broth	9.96-38.13
4-A	PFPeA, no bacteria, 3 mg/L Broth	1.46-2.40
4-P	PFPeA, *P.putida*, 3 mg/L Broth	0.67-2.15

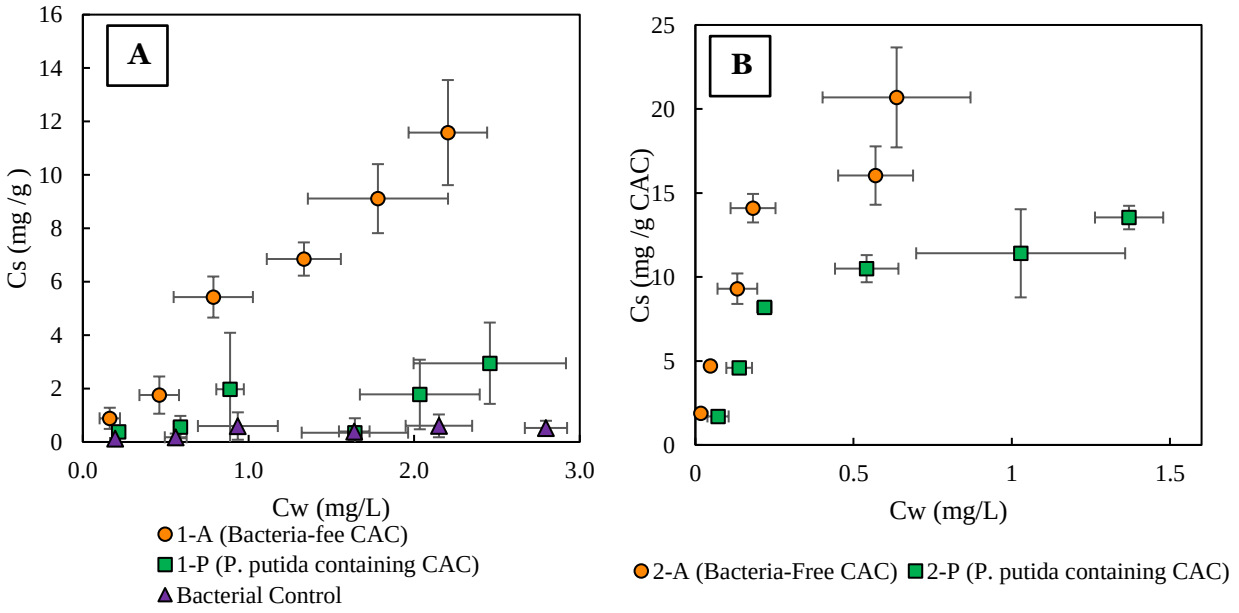


Figure 4-14: The effect of biofilm on the adsorption of PFOS to CAC. Reaction solutions contained 0.12 g/L CAC and starting concentrations of 0.26–2.5 mg/L of PFOS and (A) 80 mg/L broth and (B) 3 mg/L broth.

No statistically significant difference at a 95% confidence level was observed between PFPeA sorption with and without biofilm. K_d value ranged from 1.46 to 2.40 L/g when no bacteria (4-A)

was present and from 0.67 to 2.15 L/g in the presence of *P.putida (4-P)*. Only 19% of the PFPeA added in experiment 4-A was removed and 15% in experiment 4-P. As discussed previously, the shorter fluorinated chain in PFPeA results in weaker hydrophobic interactions with the carbon surface and, therefore, reduced sorption. As the extent of PFPeA sorption is limited, no difference was observed when biofilm occupies a fraction of the available sorption sites.

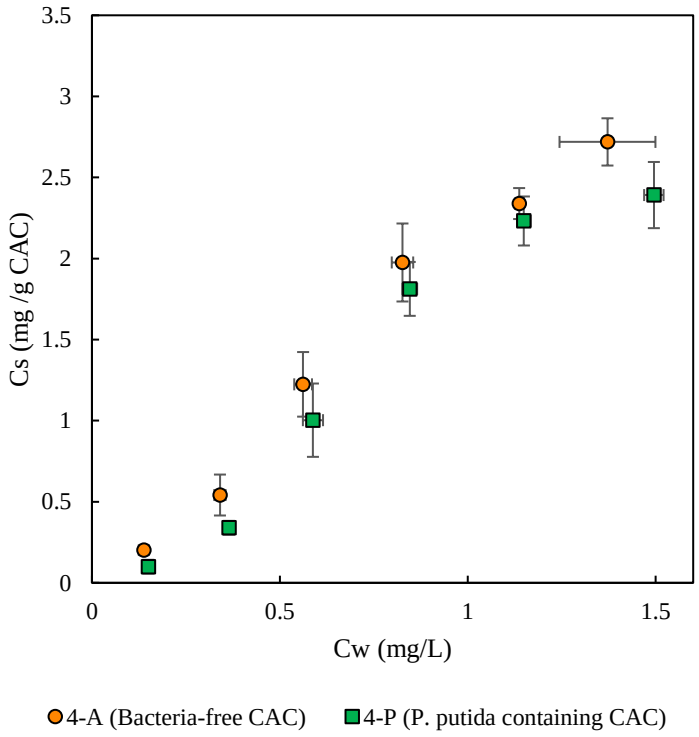


Figure 4-15: Distribution of PFPeA between aqueous phase and CAC after three days for biofilm-free and biofilm-coated CAC. Error bars represent one standard deviation.

Three-day adsorption results were consistent with those obtained from kinetic experiments. A statistically significant difference in PFOS sorption was present for bacteria-free and *P.putida*-containing CAC in microcosms with 80 mg/L and 3 mg/L starting broth concentration. Differences in microcosm pH were considered as a contributing factor to the observed difference in sorption. Further study into the effect of pH on PFAS sorption to CAC is required but, in a study

conducted by Qian et al. (2017), PAC was shown to sorb 1.2 mg/m^2 of PFOS at a pH of 6 and 1.0 mg/m^2 of PFOS at a pH of 8, equating to a 18% difference between the two conditions (Qian et al., 2017). Between the bacteria-free and *P.putida*-containing CAC experiments conducted, a percent difference in PFOS sorption of 119% occurred in 80 mg/L broth experiments and 42% in the 3 mg/L broth microcosms. The larger difference in sorbed PFOS concentration in the bacteria-free (pH of 7) and *P.putida*-containing (pH of 8.5) experiments indicates that the pH difference may not fully account for the observed decrease in sorption. The blocking of available sorption sites by the biofilm is likely to be a more prominent factor in PFOS experiments. In the experiments with PFPeA, the sorption extent was limited in both biofilm-free and *P.putida*-containing microcosms, resulting in no statistically significant difference being identified.

Chapter 5: Conclusions and Recommendations

This study aimed to enhance our understanding of how biofilms affect the adsorption of PFAS to CAC. Bench-scale experiments were conducted to evaluate the biofilm formation on colloidal-sized AC particles and its impact on the adsorption of PFOS and PFPeA. This study provide insight into how the formation of biofilms on fine particulate may decrease the adsorption rate and capacity of CAC for long chain PFAS.

CLSM images revealed that when no particulate was present, *P.putida* bacteria remained planktonic, but biofilm formation occurred when either CAC or fine sand was present. Over the course of seven days, biofilm formation on CAC was characterized by an increase in biofilm thickness and a reduction in surface roughness, suggesting a more cohesive and structured biofilm developed over time. These findings indicate that CAC provides a suitable surface for biofilm development.

Data from kinetic sorption experiments indicated that PFPeA exhibited minimal sorption to CAC, likely due to the limited hydrophobic interactions resulting from the shorter fluorinated tail. In contrast, PFOS sorption reached equilibrium within the first three days, regardless of bacterial presence. However, the formation of biofilm resulted in a reduced PFOS sorption capacity, likely due to interference with PFOS access to available sorption sites.

Three-day adsorption experiments confirmed the kinetic data, showing significant differences in PFOS sorption between bacteria-free and *P.putida*-containing CAC under both 80 mg/L and 3 mg/L broth conditions. Biofilm blockage of sorption sites appeared to be the dominant factor contributing to the reduced PFOS sorption. PFPeA, a hydrophilic compound, did not adsorb to

CAC appreciably under the conditions studied. No significant difference in PFPeA sorption was observed between the bacteria-free and biofilm-containing CAC systems.

These findings enhance our understanding of how biofilm could influence the effectiveness of CAC-based PRBs in managing PFAS contamination. For sites with a high concentration of organic carbon, the formation of bacterial biofilms may contribute to a decreased sorption capacity for long chain PFAS within a PRB.

Further research is needed to fully elucidate the effects of biofilm on PFAS sorption to CAC. In batch studies, adjustment of solution pH, use of a larger array of PFAS compounds, consideration in conjunction with other parameters and use of an anaerobic multispecies biofilm should be considered. In this study, pH variations caused by bacterial metabolism of acetate may have influenced the results, though the effect is assumed to be minimal. Future bench scale studies should control pH more rigorously throughout the experimental period to isolate its impact. Additionally, exploring a broader range of PFAS compounds, including variations in chain length and head groups, would help elucidate the role of chemical structure in PFAS-biofilm interactions. As biofilm growth may very with other groundwater parameters it may be beneficial to incorporate the study of biofilm on the sorption of PFAS to CAC into a factorial experiment. Investigating the use of anaerobic, multispecies biofilms may also improve the relevance of these findings, as limited dissolved oxygen is available in the subsurface and multiple microbial species are typically involved in the formation of biofilms. The effects of biofilm on the sorption of PFAS to CAC may also warrant larger-scale investigation, either through column studies or quantification of PRB microbiology during the field implementation for PFAS. By addressing these factors, future studies can better replicate the in-situ conditions and allow for the more accurate design of PRBs for PFAS remediation.

Citations

Abbasian Chaleshtari, Z., & Foudazi, R. (2022). A Review on Per- and Polyfluoroalkyl Substances (PFAS) Remediation: Separation Mechanisms and Molecular Interactions. *ACS ES&T Water*. https://doi.org/10.1021/acsestwater.2c00271

Aktaş, Ö., & Çeçen, F. (2007). Bioregeneration of activated carbon: A review. *International Biodeterioration & Biodegradation*, *59*(4), 257–272. https://doi.org/10.1016/J.IBIOD.2007.01.003

Allen, R. J., & Waclaw, B. (2018). Bacterial growth: a statistical physicist's guide. *Reports on Progress in Physics*, *82*(1), 016601. https://doi.org/10.1088/1361-6633/AAE546

Arena, N., Lee, J., & Clift, R. (2016). Life Cycle Assessment of activated carbon production from coconut shells. *Journal of Cleaner Production*, *125*, 68–77. https://doi.org/10.1016/J.JCLEPRO.2016.03.073

Artyushkova, K., Roizman, D., Santoro, C., Doyle, L. E., Fatima Mohidin, A., Atanassov, P., & Marsili, E. (2016). Anodic biofilms as the interphase for electroactive bacterial growth on carbon veil. *Biointerphases*, *11*(3), 031013. https://doi.org/10.1116/1.4962264

ATCC. (2022). *Pseudomonas putida (Trevisan) Migula 12633 ™*. www.atcc.org

Ateia, M., Maroli, A., Tharayil, N., & Karanfil, T. (2019). The overlooked short- and ultrashort-chain poly- and perfluorinated substances: A review. *Chemosphere*, *220*, 866–882. https://doi.org/10.1016/J.CHEMOSPHERE.2018.12.186

Azeredo, J., Azevedo, N. F., Briandet, R., Cerca, N., Coenye, T., Costa, A. R., Desvaux, M., Di Bonaventura, G., Hébraud, M., Jaglic, Z., Kačániová, M., Knøchel, S., Lourenço, A., Mergulhão, F., Meyer, R. L., Nychas, G., Simões, M., Tresse, O., & Sternberg, C. (2017). Critical review on biofilm methods. *Critical Reviews in Microbiology*, *43*(3), 313–351. https://doi.org/10.1080/1040841X.2016.1208146

Barzen-Hanson, K. A., Roberts, S. C., Choyke, S., Oetjen, K., McAlees, A., Riddell, N., McCrindle, R., Ferguson, P. L., Higgins, C. P., & Field, J. A. (2017). Discovery of 40 Classes of Per- and Polyfluoroalkyl Substances in Historical Aqueous Film-Forming Foams (AFFFs) and AFFF-Impacted Groundwater. *Environmental Science and Technology*, *51*(4), 2047–2057. https://doi.org/10.1021/ACS.EST.6B05843/SUPPL_FILE/ES6B05843_SI_002.XLSX

Bester, E., Edwards, E. A., & Wolfaardt, G. M. (2009). Planktonic cell yield is linked to biofilm development. *Can. J. Microbiol*, *55*, 1195–1206. https://doi.org/10.1139/W09-075

Beyenal, H., Donovan, C., Lewandowski, Z., & Harkin, G. (2004). Three-dimensional biofilm structure quantification. *Journal of Microbiological Methods*, *59*(3), 395–413. https://doi.org/10.1016/j.mimet.2004.08.003

Birnstingl, J., & Wilson, J. (2024). A Cost Comparison of Pump-and-Treat and In Situ Colloidal Activated Carbon for PFAS Plume Management. *Remediation Journal*, *35*(1), e70005. https://doi.org/10.1002/REM.70005

Bonaglia, S., Broman, E., Brindefalk, B., Hedlund, E., Hjorth, T., Rolff, C., Nascimento, F. J. A., Udekwu, K., & Gunnarsson, J. S. (2020). Activated carbon stimulates microbial diversity and PAH biodegradation under anaerobic conditions in oil-polluted sediments. *Chemosphere*, *248*. https://doi.org/10.1016/j.chemosphere.2020.126023

Brusseau, M. L., Anderson, R. H., & Guo, B. (2020). PFAS concentrations in soils: Background levels versus contaminated sites. *Science of The Total Environment*, *740*, 140017. https://doi.org/10.1016/J.SCITOTENV.2020.140017

Buck, R. C., Franklin, J., Berger, U., Conder, J. M., Cousins, I. T., Voogt, P. De, Jensen, A. A., Kannan, K., Mabury, S. A., & van Leeuwen, S. P. J. (2011). Perfluoroalkyl and polyfluoroalkyl substances in the environment: Terminology, classification, and origins. *Integrated Environmental Assessment and Management*, *7*(4), 513–541. https://doi.org/10.1002/IEAM.258

Butzen, M. L., Wilkinson, J. T., Mcguinness, S. R., Amezquita, S., Peaslee, G. F., & Fein, J. B. (2020). Sorption and desorption behavior of PFOS and PFOA onto a Gram-positive and a Gram-negative bacterial species measured using particle-induced gamma-ray emission (PIGE) spectroscopy. *Chemical Geology*, *552*. https://doi.org/10.1016/j.chemgeo.2020.119778

Cai, W., Navarro, D. A., Du, J., Ying, G., Yang, B., McLaughlin, M. J., & Kookana, R. S. (2022). Increasing ionic strength and valency of cations enhance sorption through hydrophobic interactions of PFAS with soil surfaces. *Science of The Total Environment*, *817*, 152975. https://doi.org/10.1016/J.SCITOTENV.2022.152975

Carey, G. R., Hakimabadi, S. G., Singh, M., McGregor, R., Woodfield, C., Van Geel, P. J., & Pham, A. L. T. (2022). Longevity of colloidal activated carbon for in situ PFAS remediation at AFFF-contaminated airport sites. *Remediation Journal*, *33*(1), 3–23. https://doi.org/10.1002/REM.21741

Carl Zeiss MicroImaging GmbH. (2011). *LSM 700 Operating Manual*.

Çeçen, F., & Aktaş, Ö. (2011). *Activated Carbon for Water and Wastewater Treatment*. Wiley-VCH.

Chen, W., Zhang, X., Mamadiev, M., & Wang, Z. (2017). Sorption of perfluorooctane sulfonate and perfluorooctanoate on polyacrylonitrile fiber-derived activated carbon fibers: in comparison with activated carbon. *RSC Advances*, *7*(2), 927–938. https://doi.org/10.1039/C6RA25230C

Dai, M., Yan, N., & Brusseau, M. L. (2023). Potential impact of bacteria on the transport of PFAS in porous media. *Water Research*, *243*. https://doi.org/10.1016/j.watres.2023.120350

Dalahmeh, S. S., Alziq, N., & Ahrens, L. (2019). Potential of biochar filters for onsite wastewater treatment: Effects of active and inactive biofilms on adsorption of per-and polyfluoroalkyl

substances in laboratory column experiments. *Environmental Pollution*, *247*, 155–164. https://doi.org/10.1016/j.envpol.2019.01.032

D'ambro, E. L., Pye, H. O. T., Bash, J. O., Bowyer, J., Allen, C., Efstathiou, C., Gilliam, R. C., Reynolds, L., Talgo, K., & Murphy, B. N. (2021). Characterizing the Air Emissions, Transport, and Deposition of Per-and Polyfluoroalkyl Substances from a Fluoropolymer Manufacturing Facility. *Cite This: Environ. Sci. Technol*, *55*. https://doi.org/10.1021/acs.est.0c06580

De Silva, A. O., Armitage, J. M., Bruton, T. A., Dassuncao, C., Heiger-Bernays, W., Hu, X. C., Kärrman, A., Kelly, B., Ng, C., Robuck, A., Sun, M., Webster, T. F., & Sunderland, E. M. (2021). PFAS Exposure Pathways for Humans and Wildlife: A Synthesis of Current Knowledge and Key Gaps in Understanding. *Environmental Toxicology and Chemistry*, *40*(3), 631–657. https://doi.org/10.1002/ETC.4935

Du, Z., Deng, S., Bei, Y., Huang, Q., Wang, B., Huang, J., & Yu, G. (2014). Adsorption behavior and mechanism of perfluorinated compounds on various adsorbents-A review. *Journal of Hazardous Materials*, *274*, 443–454. https://doi.org/10.1016/j.jhazmat.2014.04.038

Erkoc, S., & Erkoc, F. (2001). Structural and electronic properties of PFOS and LiPFOS. *Thermo Chem*, *549*, 289–293. www.elsevier.com/locate/theochem

Evich, M. G., Davis, M. J. B., McCord, J. P., Acrey, B., Awkerman, J. A., Knappe, D. R. U., Lindstrom, A. B., Speth, T. F., Tebes-Stevens, C., Strynar, M. J., Wang, Z., Weber, E. J., Henderson, W. M., & Washington, J. W. (2022). Per- and polyfluoroalkyl substances in the environment. *Science*, *375*(6580). https://doi.org/10.1126/SCIENCE.ABG9065/ASSET/9B850934-881E-40FD-8450-8FEFADB07894/ASSETS/IMAGES/LARGE/SCIENCE.ABG9065-F6.JPG

Fan, D., Gilbert, E. J., & Fox, T. (2017). Current state of in situ subsurface remediation by activated carbon-based amendments. *Journal of Environmental Management*, *204*, 793–803. https://doi.org/10.1016/j.jenvman.2017.02.014

Fenton, S. E., Ducatman, A., Boobis, A., DeWitt, J. C., Lau, C., Ng, C., Smith, J. S., & Roberts, S. M. (2021). Per- and Polyfluoroalkyl Substance Toxicity and Human Health Review: Current State of Knowledge and Strategies for Informing Future Research. *Environmental Toxicology and Chemistry*, *40*(3), 606–630. https://doi.org/10.1002/ETC.4890

Ferreira, T., & Rasband, W. (2012). *ImageJ User Guide IJ 1.46r*. http://fiji.sc/guide.git.

Fitzgerald, N. J. M., Wargenau, A., Sorenson, C., Pedersen, J., Tufenkji, N., Novak, P. J., & Simcik, M. F. (2018). Partitioning and Accumulation of Perfluoroalkyl Substances in Model Lipid Bilayers and Bacteria. *Environmental Science and Technology*, *52*(18), 10433–10440. https://doi.org/10.1021/ACS.EST.8B02912/SUPPL_FILE/ES8B02912_SI_001.PDF

Flemming, H.-C., & Wingender, J. (2010). The biofilm matrix. *Nature Reviews Microbiology*, *8*, 623–633. https://doi.org/10.1038/nrmicro2415

Fu, J., Gao, B., Xu, H., Hao, S., Ren, J., Wu, J., & Sun, Y. (2023). Effects of biofilms on the retention and transport of PFOA in saturated porous media. *Journal of Hazardous Materials*, *443*, 130392. https://doi.org/10.1016/j.jhazmat.2022.130392

Gavaskar, A. R. (1999). Design and construction techniques for permeable reactive barriers. *Journal of Hazardous Materials*, *68*(1–2), 41–71. https://doi.org/10.1016/S0304-3894(99)00031-X

Gebregiorgis Ambaye, T., Vaccari, M., Prasad, S., & Rtimi, S. (2022). Recent progress and challenges on the removal of per- and poly-fluoroalkyl substances (PFAS) from contaminated soil and water. *Environmental Science and Pollution Research*, *29*, 58405–58428. https://doi.org/10.1007/s11356-022-21513-2

Giesy, J. P., & Kannan, K. (2001). Global distribution of perfluorooctane sulfonate in wildlife. *Environmental Science and Technology*, *35*(7), 1339–1342. https://doi.org/10.1021/ES001834K/ASSET/IMAGES/LARGE/ES001834KF00002.JPEG

Gilak Hakimabadi, S. (2024). *An Investigation of Factors Affecting the Adsorption of Per-and Polyfluoroalkyl Substances (PFAS) on Colloidal Activated Carbon (CAC): Implications for In-situ Immobilization of PFAS by CAC Barriers*.

Gilak Hakimabadi, S., Taylor, A., & Le-Tuan Pham, A. (2023). Factors Affecting the Adsorption of Per-and Polyfluoroalkyl Substances (PFAS) by Colloidal Activated Carbon. *Water Research*. https://doi.org/10.1016/j.watres.2023.120212

Gjermansen, M., Ragas, P., Sternberg, C., Molin, S., & Tolker-Nielsen, T. (2005). Characterization of starvation-induced dispersion in Pseudomonas putida biofilms. *Environmental Microbiology*, *7*(6), 894–904. https://doi.org/10.1111/J.1462-2920.2005.00775.X

Glüge, J., Scheringer, M., Cousins, I. T., Dewitt, J. C., Goldenman, G., Herzke, D., Lohmann, R., Ng, C. A., Trier, X., & Wang, Z. (2020). An overview of the uses of per- and polyfluoroalkyl substances (PFAS). *Environmental Science: Processes & Impacts*, *22*(12), 2345–2373. https://doi.org/10.1039/D0EM00291G

Grieco, S. A., Chang, J., Maio, E. Y., & Hwang, M. (2021). Comparing conventional and emerging adsorbents for per- and polyfluoroalkyl substances: Kinetic, equilibrium, and column experiments. *AWWA Water Science*, *3*(6), e1256. https://doi.org/10.1002/AWS2.1256

Heydorn, A., Nielsen, A. T., Hentzer, M., Sternberg, C., Givskov, M., Ersboll, B. K., & Molin, S. (2000). Quantification of biofilm structures by the novel computer program COMSTAT. *Microbiology*, *146*(10), 2395–2407. https://doi.org/10.1099/00221287-146-10-2395/CITE/REFWORKS

Hort, H. M., Robinson, C. E., Sawyer, A. H., Li, Y., Cardoso, R., Lee, S. A., Roff, D., Adamson, D. T., & Newell, C. J. (2024). Conceptualizing Controlling Factors for PFAS Salting Out in Groundwater Discharge Zones Along Sandy Beaches. *Groundwater*. https://doi.org/10.1111/GWAT.13428

Hu, X. C., Andrews, D. Q., Lindstrom, A. B., Bruton, T. A., Schaider, L. A., Grandjean, P., Lohmann, R., Carignan, C. C., Blum, A., Balan, S. A., Higgins, C. P., Sunderland, E. M., John, H., & Paulson, A. (2016). *Detection of Poly-and Perfluoroalkyl Substances (PFASs) in U.S. Drinking Water Linked to Industrial Sites, Military Fire Training Areas, and Wastewater Treatment Plants*. https://doi.org/10.1021/acs.estlett.6b00260

Hu, X. C., Tokranov, A. K., Liddie, J., Zhang, X., Grandjean, P., Hart, J. E., Laden, F., Sun, Q., Yeung, L. W. Y., & Sunderland, E. M. (2019). Tap water contributions to plasma concentrations of poly- and perfluoroalkyl substances (PFAS) in a nationwide prospective cohort of U.S. women. *Environmental Health Perspectives*, *127*(6). https://doi.org/10.1289/EHP4093

Invitrogen. (2006). *Concanavalin A Conjugates*.

Jeirani, Z., Niu, C. H., & Soltan, J. (2017). Adsorption of emerging pollutants on activated carbon. *Reviews in Chemical Engineering*, *33*(5), 491–522. https://doi.org/10.1515/REVCE-2016-0027

Jian, J. M., Chen, D., Han, F. J., Guo, Y., Zeng, L., Lu, X., & Wang, F. (2018). A short review on human exposure to and tissue distribution of per- and polyfluoroalkyl substances (PFASs). *Science of The Total Environment*, *636*, 1058–1069. https://doi.org/10.1016/J.SCITOTENV.2018.04.380

Johnson, G. R., Brusseau, M. L., Carroll, K. C., Tick, G. R., & Duncan, C. M. (2022). Global distributions, source-type dependencies, and concentration ranges of per- and polyfluoroalkyl substances in groundwater. *Science of The Total Environment*, *841*, 156602. https://doi.org/10.1016/J.SCITOTENV.2022.156602

Kim, G., Mengesha, D. N., & Choi, Y. (2024). Adsorption dynamics of per-and polyfluoroalkyl substances (PFAS) on activated carbon: Interplay of surface chemistry and PFAS structural

properties. *Separation and Purification Technology*, *349*, 1383–5866. https://doi.org/10.1016/j.seppur.2024.127851

Kim, Y., Park, S., & Oh, S. (2021). Machine learning approach reveals the assembly of activated sludge microbiome with different carbon sources during microcosm startup. *Microorganisms*, *9*(7), 1387. https://doi.org/10.3390/MICROORGANISMS9071387/S1

Kivisaar, M. (2020). Narrative of a versatile and adept species Pseudomonas putida. *Journal of Medical Microbiology*, *69*, 324–338. https://doi.org/10.1099/jmm.0.001137

Koch, A. L. (1970). Turbidity Measurements of Bacterial Cultures in Some Available Commercial Instruments. *Analytical Biochemistry*, *38*, 252–259.

Kumar Pramanik, B., Kumar Pramanik, S., Sarker, C., & Suja, F. (2016). *Removal of emerging perfluorooctanoic acid and perfluorooctane sulfonate contaminants from lake water*. https://doi.org/10.1080/09593330.2016.1240716

Labauve, A. E., & Wargo, M. J. (2012). Growth and Laboratory Maintenance of Pseudomonas aeruginosa. *Curr Protoc Microbiol*. https://doi.org/10.1002/9780471729259.mc06e01s25

Life Technologies. (2014). *SYTO ® Green-Fluorescent Nucleic Acid Stains*.

Linkert, M., Rueden, C. T., Allan, C., Burel, J. M., Moore, W., Patterson, A., Loranger, B., Moore, J., Neves, C., MacDonald, D., Tarkowska, A., Sticco, C., Hill, E., Rossner, M., Eliceiri, K. W., & Swedlow, J. R. (2010). Metadata matters: access to image data in the real world. *Journal of Cell Biology*, *189*(5), 777–782. https://doi.org/10.1083/JCB.201004104

Mccleaf, P., Englund, S., Ostlund, A. €, Lindegren, K., Wiberg, K., & Ahrens, L. (2017). Removal efficiency of multiple poly- and perfluoroalkyl substances (PFASs) in drinking water using granular activated carbon (GAC) and anion exchange (AE) column tests. *Water Research*, *120*, 77–87. https://doi.org/10.1016/j.watres.2017.04.057

Mcdonough, K. M., Fairey, J. L., & Lowry, G. V. (2007). *Adsorption of polychlorinated biphenyls to activated carbon: Equilibrium isotherms and a preliminary assessment of the effect of*

dissolved organic matter and biofilm loadings. https://doi.org/10.1016/j.watres.2007.07.053

McGarr, J. T., Mbonimpa, E. G., McAvoy, D. C., & Soltanian, M. R. (2023). Fate and Transport of Per- and Polyfluoroalkyl Substances (PFAS) at Aqueous Film Forming Foam (AFFF) Discharge Sites: A Review. *Soil Systems*, *7*(2), 53. https://doi.org/10.3390/SOILSYSTEMS7020053/S1

McGregor, R. (2018). In Situ treatment of PFAS-impacted groundwater using colloidal activated Carbon. *Remediation Journal*, *28*(3), 33–41. https://doi.org/10.1002/REM.21558

McGregor, R. (2020a). Distribution of Colloidal and Powdered Activated Carbon for the in Situ Treatment of Groundwater. *Journal of Water Resource and Protection*, *12*, 1001–1018. https://doi.org/10.4236/jwarp.2020.1212060

McGregor, R. (2020b). Six pilot-scale studies evaluating the in situ treatment of PFAS in groundwater. *Remediation Journal*, *30*(3), 39–50. https://doi.org/10.1002/REM.21653

McGregor, R., & Benevenuto, L. (2021). The Effect of Heterogeneity on the Distribution and Treatment of PFAS in a Complex Geologic Environment. *Frontiers in Environmental Chemistry*, *2*, 729779. https://doi.org/10.3389/FENVC.2021.729779

Milley, S. A., Koch, I., Fortin, P., Archer, J., Reynolds, D., & Weber, K. P. (2018). Estimating the number of airports potentially contaminated with perfluoroalkyl and polyfluoroalkyl substances from aqueous film forming foam: A Canadian example. *Journal of Environmental Management*, *222*, 122–131. https://doi.org/10.1016/j.jenvman.2018.05.028

Minh, T., Nguyen, H., Brä, J., Thompson, K., Thompson, J., Kabiri, S., Navarro, D. A., Kookana, R. S., Grimison, C., Barnes, C. M., Higgins, C. P., Mclaughlin, M. J., & Mueller, J. F. (2020). Influences of Chemical Properties, Soil Properties, and Solution pH on Soil–Water

Partitioning Coefficients of Per-and Polyfluoroalkyl Substances (PFASs). *Cite This: Environ. Sci. Technol*, *54*, 15883–15892. https://doi.org/10.1021/acs.est.0c05705

Molé, R. A., Velosa, A. C., Carey, G. R., Liu, X., Li, G., Fan, D., Danko, A., & Lowry, G. V. (2024). Groundwater solutes influence the adsorption of short-chain perfluoroalkyl acids (PFAA) to colloidal activated carbon and impact performance for in situ groundwater remediation. *Journal of Hazardous Materials*, *474*, 134746. https://doi.org/10.1016/J.JHAZMAT.2024.134746

Ndubueze, E. U., Boparai, H. K., Xu, L., & Sleep, B. E. (2024). Colloidal properties and stability of colloidal activated carbon: effects of aqueous chemistry on sedimentation kinetics. *Environmental Science: Nano*. https://doi.org/10.1039/D4EN00572D

Niarchos, G., Ahrens, L., Kleja, D. B., & Fagerlund, F. (2022). Per- and polyfluoroalkyl substance (PFAS) retention by colloidal activated carbon (CAC) using dynamic column experiments. *Environmental Pollution*, *308*, 119667. https://doi.org/10.1016/J.ENVPOL.2022.119667

Niarchos, G., Ahrens, L., Kleja, D. B., Leonard, G., Forde, J., Bergman, J., Ribeli, E., Schütz, M., & Fagerlund, F. (2023). In-situ application of colloidal activated carbon for PFAS-contaminated soil and groundwater: A Swedish case study. *Remediation Journal*, *33*(2), 101–110. https://doi.org/10.1002/REM.21746

Nilsson, H., Karrman, A., Westberg, H., Rotander, A., Van Bavel, B., & Lindström, G. (2010). A time trend study of significantly elevated perfluorocarboxylate levels in humans after using fluorinated ski wax. *Environmental Science and Technology*, *44*(6), 2150–2155. https://doi.org/10.1021/ES9034733/SUPPL_FILE/ES9034733_SI_001.PDF

Obiri-Nyarko, F., Grajales-Mesa, S. J., & Malina, G. (2014). *An overview of permeable reactive barriers for in situ sustainable groundwater remediation*. https://doi.org/10.1016/j.chemosphere.2014.03.112

O'Toole, G., Kaplan, H. B., & Kolter, R. (2000). Biofilm Formation as Microbial Development. *Annu Rev. Microbiol*, *54*, 49–79. https://doi.org/10.1146/ANNUREV.MICRO.54.1.49

Probandt, D., Eickhorst, T., Ellrott, A., Amann, R., & Knittel, K. (2017). Microbial life on a sand grain: from bulk sediment to single grains. *The ISME Journal 2018 12:2*, *12*(2), 623–633. https://doi.org/10.1038/ismej.2017.197

Qian, J., Shen, M., Wang, P., Wang, C., Li, K., Liu, J., Lu, B., & Tian, X. (2017). Perfluorooctane sulfonate adsorption on powder activated carbon: Effect of phosphate (P) competition, pH, and temperature. *Chemosphere*, *182*, 215–222. https://doi.org/10.1016/J.CHEMOSPHERE.2017.05.033

Regenesis. (2023). *Laboratory and Field Results Documenting The Biodegradation of Contaminants From Colloidal Activated Carbon (CAC)*.

Renner, L. D., & Weibel, D. B. (2011). Physicochemical regulation of biofilm formation. *MRS Bulletin*, *36*(5), 347–355. https://doi.org/10.1557/MRS.2011.65/FIGURES/5

Rocha Díaz De León, G. R. (2021). *Impact of Anaerobic Biofilm Formation on Sorption Characteristics of Powdered Activated Carbon*. University of Waterloo.

Saeidi, N., Kopinke, F.-D., & Georgi, A. (2020). Understanding the effect of carbon surface chemistry on adsorption of perfluorinated alkyl substances. *Chemical Engineering Journal*, *381*. https://doi.org/10.1016/j.cej.2019.122689

Sakr, M., El Agamawi, H., Klammler, H., & Mohamed, M. M. (2023). A review on the use of permeable reactive barriers as an effective technique for groundwater remediation. *Groundwater for Sustainable Development*, *21*, 100914. https://doi.org/10.1016/J.GSD.2023.100914

Sánchez-Clemente, R., Guijo, M. I., Nogales, J., & Blasco, R. (2020). Carbon Source Influence on Extracellular pH Changes along Bacterial Cell-Growth. *Genes 2020, Vol. 11, Page 1292*, *11*(11), 1292. https://doi.org/10.3390/GENES11111292

Scherer, M. M., Richter, S., Valentine, R. L., & Alvarez, P. J. J. (2000). Chemistry and Microbiology of Permeable Reactive Barriers for In Situ Groundwater Clean up. *Critical Reviews in Environmental Science and Technology*, *30*(3), 363–411. https://doi.org/10.1080/10643380091184219

Schlafer, S., & Meyer, R. L. (2017). Confocal microscopy imaging of the biofilm matrix. *Journal of Microbiological Methods*, *138*, 50–59. https://doi.org/10.1016/J.MIMET.2016.03.002

Scholz, M., & Martin, R. J. (1997). ECOLOGICAL EQUILIBRIUM ON BIOLOGICAL ACTIVATED CARBON. *Wat. Res*, *31*(12), 2959–2968.

Sekar, R., Griebe, T., & Flemming, H.-C. (2002). Influence of Image Acquisition Parameters on Quantitative Measurements of Biofilms using Confocal Laser Scanning Microscopy. *Biofouling*, *18*(1), 47–56. https://doi.org/10.1080/08927010290017725

Shrout, J. D., Tolker-Nielsen, T., Givskov, M., & Parsek, M. R. (2011). The contribution of cell-cell signaling and motility to bacterial biofilm formation. *MRS Bulletin*, *36*(5), 367–373. https://doi.org/10.1557/MRS.2011.67

Simpson, D. R. (2008). Biofilm processes in biologically active carbon water purification. *Water Research*, *42*(12), 2839–2848. https://doi.org/10.1016/J.WATRES.2008.02.025

Sorengard, M., Berggren Kleja, D., & Ahrens, L. (2019). Stabilization of per-and polyfluoroalkyl substances (PFASs) with colloidal activated carbon (PlumeStop®) as a function of soil clay and organic matter content. *Journal of Environmental Management*. https://doi.org/10.1016/j.jenvman.2019.109345

Stewart, P. S., Murga, R., Srinivasan, R., & de Beer, D. (1995). Biofilm structural heterogeneity visualized by three microscopic methods. *Water Research*, *29*(8), 2006–2009. https://doi.org/10.1016/0043-1354(94)00339-9

Stoiber, T., Evans, S., & Naidenko, O. V. (2020). Disposal of products and materials containing per- and polyfluoroalkyl substances (PFAS): A cyclical problem. *Chemosphere*, *260*, 127659. https://doi.org/10.1016/J.CHEMOSPHERE.2020.127659

Stoodley, P., Sauer, K., Davies, D. G., & Costerton, J. W. (2002). BIOFILMS AS COMPLEX DIFFERENTIATED COMMUNITIES. *Annu. Rev. Microbiol*, *56*, 187–209. https://doi.org/10.1146/annurev.micro.56.012302.160705

Sutton, S. (2011). Measurement of Microbial Cells by Optical Density. *Journal of Validation Technology*, 46–49.

Thiruvenkatachari, R., Vigneswaran, S., & Naidu, R. (2008). Permeable reactive barrier for groundwater remediation. *Journal of Industrial and Engineering Chemistry*, *14*(2), 145–156. https://doi.org/10.1016/J.JIEC.2007.10.001

Tolker-Nielsen, T., Brinch, U. C., Ragas, P. C., Andersen, J. B., Jacobsen, C. S., & Molin, S. (2000). Development and dynamics of Pseudomonas sp. biofilms. *Journal of Bacteriology*, *182*(22), 6482–6489. https://doi.org/10.1128/JB.182.22.6482-6489.2000

Turonova, H., Neu, T. R., Ulbrich, P., Pazlarova, J., & Tresse, O. (2016). The biofilm matrix of Campylobacter jejuni determined by fluorescence lectin-binding analysis. *Biofouling*, *32*(5), 597–608. https://doi.org/10.1080/08927014.2016.1169402

Umeh, A. C., Hassan, M., Egbuatu, M., Zeng, Z., Al Amin, M., Samarasinghe, C., & Naidu, R. (2023). Multicomponent PFAS sorption and desorption in common commercial adsorbents: Kinetics, isotherm, adsorbent dose, pH, and index ion and ionic strength effects. *Science of The Total Environment*, *904*, 166568. https://doi.org/10.1016/J.SCITOTENV.2023.166568

US EPA. (2016). *Health Effects Support Document for Perfluorooctane Sulfonate (PFOS)*.

US EPA. (2018). *Activated Carbon-Based Technology for In Situ Remediation At a Glance*.

van Oss, C. J., Absolom, D. R., & Neumann, A. W. (1980). The 'hydrophobic effect': Essentially a van der Waals interaction. *Colloid and Polymer Science Kolloid Zeitschrift & Zeitschrift Für Polymere*, *258*(4), 424–427. https://doi.org/10.1007/BF01480835/METRICS

Vestergren, R., & Cousins, I. T. (2009). Tracking the pathways of human exposure to perfluorocarboxylates. *Environmental Science and Technology*, *43*(15), 5565–5575. https://doi.org/10.1021/ES900228K/SUPPL_FILE/ES900228K_SI_001.PDF

Wang, W., Rhodes, G., Zhang, W., Yu, X., Teppen, B. J., & Li, H. (2021). *Implication of cation-bridging interaction contribution to sorption of perfluoroalkyl carboxylic acids by soils*. https://doi.org/10.1016/j.chemosphere.2021.133224

Wang, Z., Dewitt, J. C., Higgins, C. P., & Cousins, I. T. (2017). A Never-Ending Story of Per- and Polyfluoroalkyl Substances (PFASs)? *Environmental Science and Technology*, *51*(5), 2508–2518. https://doi.org/10.1021/ACS.EST.6B04806/ASSET/IMAGES/LARGE/ES-2016-048069_0002.JPEG

Weathers, T. S., Higgins, C. P., & Sharp, J. O. (2015). Enhanced biofilm production by a toluene-degrading rhodococcus observed after exposure to perfluoroalkyl acids. *Environmental Science and Technology*, *49*(9), 5458–5466. https://doi.org/10.1021/ES5060034/SUPPL_FILE/ES5060034_SI_001.PDF

Wilson, C., Lukowicz, R., Merchant, S., Valquier-Flynn, H., Caballero, J., Sandoval, J., Okuom, M., Huber, C., Durham Brooks, T., Wilson, E., Clement, B., Wentworth, C. D., & Holmes, A. E. (2017). Quantitative and Qualitative Assessment Methods for Biofilm Growth: A Mini-review HHS Public Access. *Res Rev J Eng Technol*, *6*(4).

Worch, E. (2021). *Adsorption Technology in Water Treatment - Fundamentals, Processes, and Modeling* (2nd Edition). De Gruyter.

Yahya, M. A., Al-Qodah, Z., & Ngah, C. W. Z. (2015). Agricultural bio-waste materials as potential sustainable precursors used for activated carbon production: A review. *Renewable and Sustainable Energy Reviews*, *46*, 218–235. https://doi.org/10.1016/J.RSER.2015.02.051

Yan, W., Qian, T., Zhang, L., Wang, L., & Zhou, Y. (2021). Interaction of perfluorooctanoic acid with extracellular polymeric substances - Role of protein. *Journal of Hazardous Materials*, *401*, 123381. https://doi.org/10.1016/J.JHAZMAT.2020.123381

Yang, X., Beyenal, H., Harkin, G., & Lewandowski, Z. (2001). Evaluation of biofilm image thresholding methods. *Water Research*, *35*(5), 1149–1158. https://doi.org/10.1016/S0043-1354(00)00361-4

Yu, J., Lv, L., Lan, P., Zhang, S., Pan, B., & Zhang, W. (2012). Effect of effluent organic matter on the adsorption of perfluorinated compounds onto activated carbon. *Journal of Hazardous Materials*, *225–226*, 99–106. https://doi.org/10.1016/J.JHAZMAT.2012.04.073

Yu, Q., Zhang, R., Deng, S., Huang, J., & Yu, G. (2009). Sorption of perfluorooctane sulfonate and perfluorooctanoate on activated carbons and resin: Kinetic and isotherm study. *Water Research*, *43*(4), 1150–1158. https://doi.org/10.1016/j.watres.2008.12.001

Zhang, T., & Fang, H. H. P. (2001). Quantification of extracellular polymeric substances in biofilms by confocal laser scanning microscopy. *Biotechnology Letters*, *23*, 405–409.

Appendix A: Artificial Groundwater Recipe

Recipe for 1 L of AGW in Milli-Q water adapted from Bester et al. to include sodium acetate (CH3COONa) was added as a nutrient source at the concentration used by Kim et al. (Bester et al., 2009; Y. Kim et al., 2021)

Concentrated Salt Solutions

Concentrated salt solutions were prepared to maintain consistency between batches of AGW and to reduce error associated with weighing the small masses the salts required for each 1 L batch. Each stock solution was prepared separately in a 20 mL vial.

- 959 mgNH_4Cl in 20 mL of Milli-Q water to give a concentration of 49,750 mg/L
- 95.2 mg $MgCl_2$ in 20 mL of Milli-Q water to give a concentration of 4760 mg/L
- 178.2 mg $MnCl_2$ in 20 mL of Milli-Q water to give a concentration of 8910 mg/L
- 2940 mg $CaCl_2$ in 20 mL of Milli-Q water to give a concentration of 147, 020 mg/L
- 170.4 mg Na_2SO_4 in 20 mL of Milli-Q water to give a concentration of 8910 mg/L
- 140.2 NaCl in 20 mL of Milli-Q water to give a concentration of 7010 mg/L

Preparation of AGW

Add 1 mL of each concentrated stock solution and 3.45 g of sodium acetate (CH_3COONa) to a 1 L volumetric flask. Fill remaining volume with Milli-Q water (18.2 MΩ·cm, Millipore) and mix well. Measure pH and adjust as needed by addition of 0.1 M solution of sodium hydroxide. Sterilize AGW by autoclaving and allow to cool before use.

Final Salt Concentrations in AGW

- 49.75 mg/L NH_4Cl
- 4.76 mg/L $MgCl_2$
- 8.91 mg/L $MnCl_2$
- 147.02 mg/L $CaCl_2$

- 8.52 mg/L Na_2SO_4
- 7.01 mg/L NaCl
- 3.45 g/L CH_3COONa

Appendix B: Additional CLSM Images

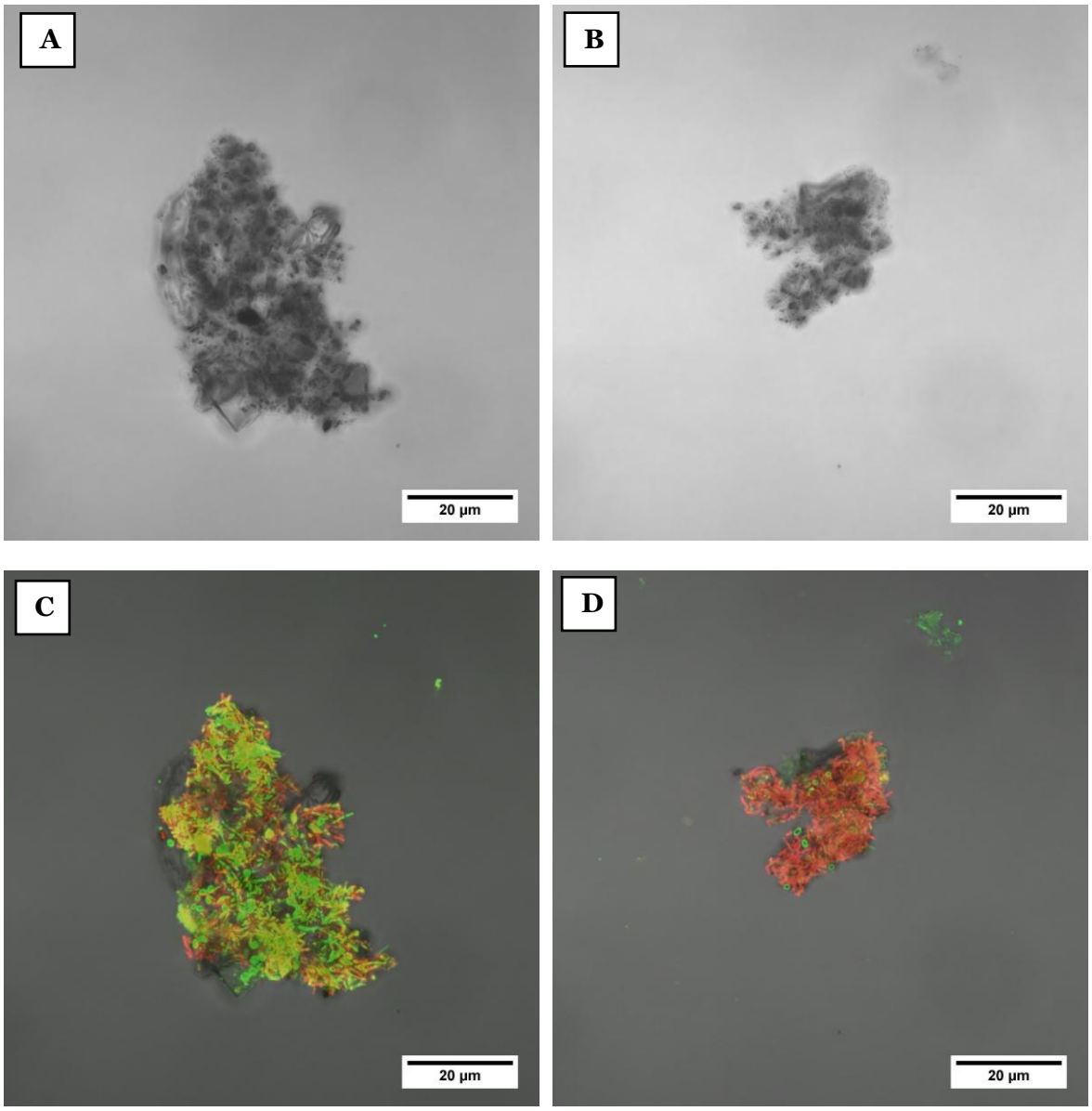


Figure 5-1: Images A and B a show visible light projections of CLSM images of bacteria coated sand. The Particulate appears as dark grey or black points and is to be embedded within the translucent grey cellular matrix. Images C and D show the visible light projections overlayed with the maximum intensity of the fluorescent dyes for P.Putida *Sand. Cells are highlighted in green and EPS is coloured red.*

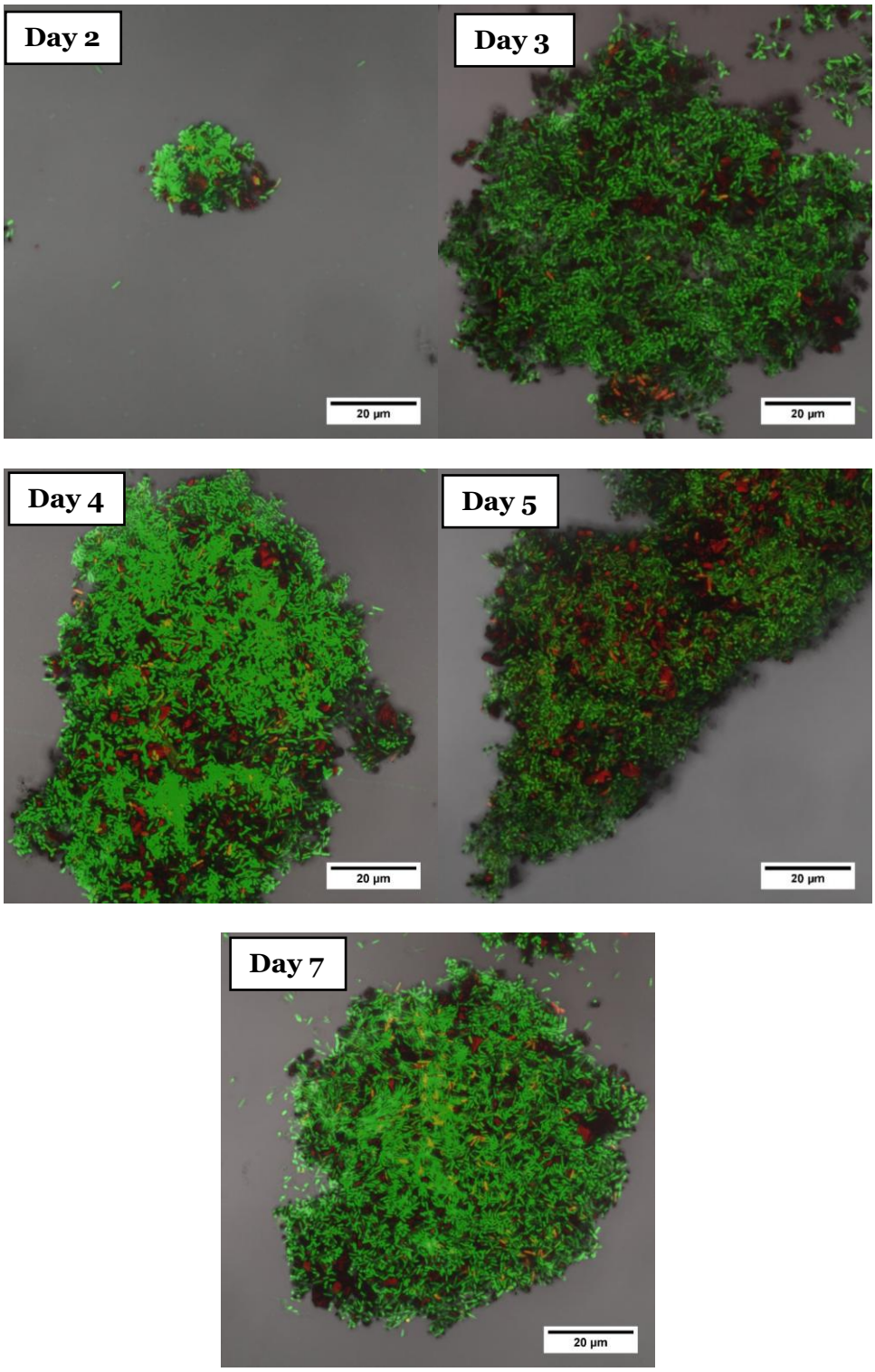


Figure 5-2: Confocal images P.putida incubated in AGW containing 30µL of CAC and 3 mg/L of broth over seven days. As samples are not returned to microcosms after microscopy, the images show separate sections of biofilm from each day. Cells are highlighted in green and EPS is coloured red.

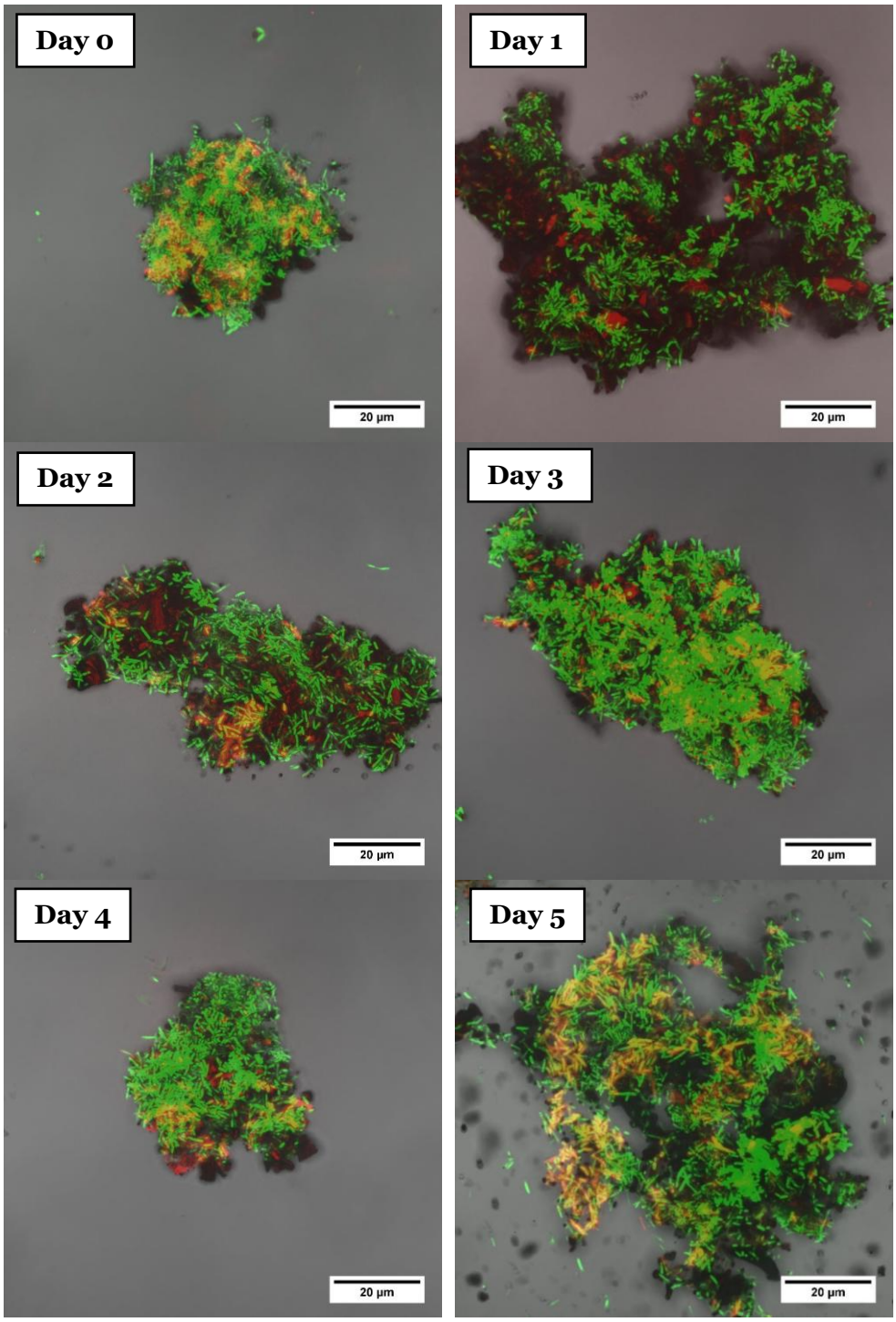


Figure 5-3: P.putida biofilm assumed to be in the stationary phase of growth over the course of five day kinetic experiment. Days are indicated as days from the addition of PFOS, day 0 is when PFOS was added, day 1 is 24 hours later, etc. As samples are not returned to microcosms after microscopy, the images show separate sections of biofilm from each day. Cells are highlighted in green and EPS is coloured red.